Goethe Universität Frankfurt am Main

Institute for Theoretical Physics

Bachelor Thesis

Gravothermal collapse of Self-Interacting Dark Matter Halos in GR

Gravothermaler Kollaps von selbstwechselwirkender Dunkle-Materie-Halos in der ART

by
Oleg Moser

Matriculation Nr.: 7196742

Submission Date: February 10, 2026

Erstgutachter: Prof. Dr. Laura Sagunski,
Zweitgutachter: Prof. Dr. Jürgen Schaffner-Bielich

Abstract

We construct a general-relativistic model of spherically symmetric self-interacting dark-matter halos based on the gravothermal fluid model, and implement it in a numerical solver. We perform simulations for several halo parameter sets and interaction cross sections, comparing an established Newtonian model with the developed relativistic model. We find that relativistic effects greatly increase the central density after gravothermal collapse, with stronger amplification for smaller self-interaction cross sections.

Zusammenfassung

Mithilfe der allgemeinen Relativitätstheorie konstruieren wir ein Modell sphärisch symmetrischer, selbstinteragierender Dunkle-Materie-Halos basierend auf dem gravothermalen Fluidmodell und implementieren es in einem numerischen Solver. Wir führen Simulationen für verschiedene Halo-Parameter und Wechselwirkungsquerschnitte durch und vergleichen ein etabliertes newtonsches Modell mit dem entwickelten relativistischen Modell. Dabei stellen wir fest, dass relativistische Effekte die zentrale Dichte nach dem gravothermischen Kollaps erheblich erhöhen, wobei die Verstärkung bei kleineren Selbstinteraktionsquerschnitten stärker ausfällt.

Danksagung

Ich bedanke mich hier herzlich bei allen, die mich während der Erstellung dieser Bachelorarbeit unterstützt und motiviert haben. Zuallererst gebührt mein aufrichtiger Dank meiner Betreuerin Prof. Laura Sagunski.

Ein besonderer Dank gilt meiner Familie, die mich während meiner gesamten Studienzeit unterstützt und ermutigt hat. Danke an meine Eltern, ihr habt immer an mich geglaubt, auch wenn ich es selbst nicht mehr tat. Danke an meine Oma, ohne die ich niemals so weit gekommen wäre. Und zu guter Letzt ein herzliches Dankeschön an meine Partnerin, die immer für mich da war und unerbittlich an meiner Seite stand.

Contents

1 Introduction

The formation and evolution of cosmic structure is described by the standard cosmological model, commonly referred to as the ΛCDM model. In this framework, the energy content of the Universe is dominated by dark energy (Λ) and cold dark matter (CDM), while baryonic matter contributes only a minor fraction. The ΛCDM model provides a successful description of the expansion history of the Universe, the cosmic microwave background, and the large-scale distribution of matter [1]. Despite its success at large scales, ΛCDM faces several issues at or below galactic scales. In particular, numerical simulations of collisionless CDM predict steep central density cusps in dark matter halos, while observations of dwarf galaxies favor isothermal cores. This discrepancy is commonly referred to as the core-cusp problem. Another issue is the missing-satellite problem, in which CDM predicts an overabundance of subhalos in the Milky Way that have not been found [2]. A proposed solution to these problems was self-interacting dark matter (SIDM), which introduced a non-vanishing interaction cross-section and, as the name suggests, allows dark matter particles to interact with each other [3]. High-resolution N-body simulations are commonly used to study the evolution of SIDM halos. A computationally cheaper approach is the semi-analytical gravothermal fluid approximation, which uses the conservation of mass, hydrostatic equilibrium, heat conduction, and the laws of thermodynamics to model a spherically symmetric SIDM halo [4]. This thesis constructs a theoretical and numerical adaptation of the evolution code developed by Boddy [5, 6] to incorporate general-relativistic equations. An open-source reference implementation by the original authors is available at `https://github.com/kboddy/GravothermalSIDM`. The primary assumption is that hydrostatic equilibrium in this system can be modeled using the Tolman-Oppenheimer-Volkoff (TOV) equations [7, 8], following the approach of Shapiro [9]. Adapting the code requires modifications to three distinct components: Initial Conditions, Hydrostatic Adjustment, and Heat Conduction. The discussion begins with an overview of cold dark matter and self-interacting dark matter. Subsequently, the equations governing the Newtonian gravothermal fluid are introduced, followed by an overview of General Relativity (GR) and the Tolman-Oppenheimer-Volkoff equations, which are used to derive the relativistic expressions for the gravothermal fluid. The numerical implementation of these equations within the existing code is then detailed. Finally, simulation results are presented and compared to the Newtonian case. The source code used to generate all results presented in this thesis is publicly available at `https://github.com/AluminiumBromid/GravothermalSIDM-GR`.

2 Cosmology

The fundamental idea in cosmology is the *cosmological principle*, which states that the Universe is statistically homogeneous and isotropic on sufficiently large scales. Under this assumption, the spacetime geometry is described by the Friedmann-Lemaître-Robertson-Walker (FLRW) metric, which represents the most general solution of Einstein's field equations consistent with these symmetries [1]. Observations of the Cosmic Microwave Background (CMB) anisotropies and large-scale structure indicate that the spatial curvature of the Universe is very close to zero, implying a spatially flat geometry to high precision [10].

The standard cosmological model, known as the ΛCDM model, describes the energy content of the Universe in terms of four main components: dark energy (represented by

the cosmological constant Λ), cold dark matter (CDM), ordinary baryonic matter, and radiation. Each component contributes differently to the cosmic expansion and evolves distinctively with the scale factor $a(t)$.

A central prediction of the FLRW spacetime is that the Universe is expanding. Due to the finite speed of light, observing distant astrophysical objects is equivalent to observing the Universe at earlier stages of its evolution. Extrapolating this expansion backward in time suggests that the primordial universe was extremely dense. The standard cosmological model postulates a singularity that led to the expansion of the universe 13.7 billion years ago, known as the Big Bang. It was followed up by an accelerated expansion called the Inflation. The oldest electromagnetic radiation observable today is the Cosmic Microwave Background. The CMB originates from the epoch of recombination, which occurred approximately 380 000 years after the Big Bang, corresponding to a redshift of $z \simeq 1100$. At this time, the Universe had expanded and cooled enough for protons and electrons to form neutral hydrogen, making the Universe transparent to photons [1]. These photons have since been redshifted by cosmic expansion and are observed today as an almost perfectly isotropic blackbody spectrum with a temperature of $T_{\mathrm{CMB}} = 2.725\,\mathrm{K}$ [11].

2.1 Cold Dark Matter

Dark matter plays a central role in this cosmological framework. Although it does not interact electromagnetically and is therefore invisible to direct observation, its gravitational effects are essential to the formation of cosmic structure. Current observations indicate that the total matter content of the Universe accounts for approximately 31% of the total energy density, while dark energy contributes about 69% [10]. Of the matter component, only about 5% consists of ordinary baryonic matter, which interacts via the electromagnetic, strong, and weak forces. The remaining $\sim 26\%$ is attributed to dark matter, which interacts predominantly through gravity. The presence of dark matter is fundamental for explaining the formation of structure in the Universe. Because baryonic matter was tightly coupled to radiation before recombination, density perturbations in the baryonic component could not grow efficiently at early times. The term "cold" denotes that dark matter particles are non-relativistic during structure formation. This enables early clumping of CDM into gravity wells, providing the seeds into which baryonic matter later fell after recombination. Without cold dark matter, the observed abundance of galaxies and large-scale structures would be difficult to explain with the age of the Universe [1].

The ΛCDM model is strongly supported by a wide range of independent observations, including measurements of the CMB, baryon acoustic oscillations, Type Ia supernovae, galaxy clustering, and gravitational lensing. These probes consistently result in the same ratio of dark matter to baryonic matter, giving strong evidence for the existence of dark matter as a fundamental component of the Universe [12].

2.1.1 Core-Cusp Problem

Comprehensive N-Body simulations by Navarro, Frenk, and White show that ΛCDM halos can generally be described by a density profile, which diverges in the centre, known as the NFW Profile

$$\rho_{\mathrm{NFW}} = \frac{\rho_s}{\frac{r}{r_s}\left(1+\frac{r}{r_s}\right)^2}, \tag{1}$$

where r_s and ρ_s are the characteristic radius and density [13]. The density in the centre is roughly $\rho \propto r^{-\alpha}$ with $\alpha = 1$. This steep density spike is called a 'cusp'. Observations of dark matter halos around dwarf galaxies instead suggest a 'cored' density profile with constant density $\alpha \approx 0$ in the core [14]. This is called the core-cusp problem. Recent simulations that include baryonic feedback [15] produce inner slopes of $\alpha = 0.4 \pm 0.1$, which are broadly consistent with observational results such as those from 'The HI Nearby Galaxy Survey' (THINGS), which finds $\alpha = 0.29 \pm 0.07$ [16].

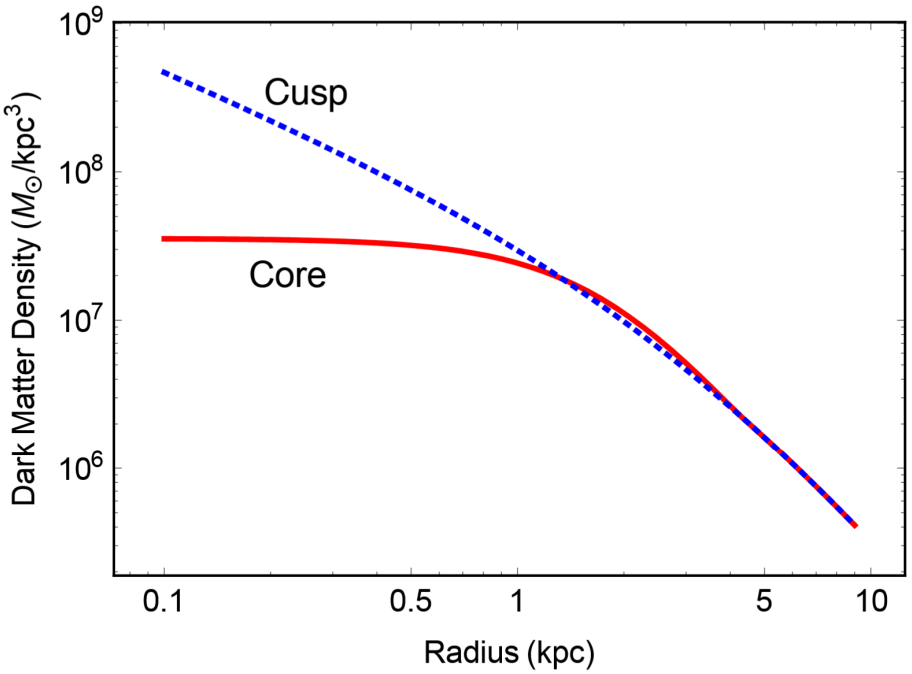

Figure 1: Density as a function of radius. The blue dotted line represents the density profile with a cusp as in NFW. The solid red line shows a cored profile. Reproduced from Fig. 4 Ref. [2].

.

2.2 Self-Interacting Dark Matter

To address the core-cusp and missing-satellite problems, Spergel & Steinhardt proposed extending CDM by introducing a non-vanishing interaction cross-section σ and allowing dark matter particles to scatter elastically with themselves [3]. The interaction strength is commonly expressed as the cross section per unit mass, $\sigma_m = \sigma/m$. The density profile in SIDM naturally produces isothermal cores, making it a good candidate for solving the Core-Cusp problem. For sufficiently small values of σ_m, SIDM behaves indistinguishably from CDM on cosmological scales, preserving the successful predictions of ΛCDM [2].

2.2.1 Gravothermal Collapse of SIDM halos

A gravitationally bound system has negative heat capacity, meaning that it heats up if it loses energy. Imagine a system with a relatively compact hot core and an extended cold outer region, then transferring heat outward heats the core even more. The increased kinetic energy is supplied by the core's potential energy, creating a runaway effect that

catastrophically raises its density and temperature while reducing its size and mass. This effect is called gravothermal collapse [17].

A characteristic feature of CDM halos is that, despite their steep central density profiles, the velocity dispersion (i.e., temperature) decreases toward the center, resulting in a cold core. Therefore, when starting with a cuspy profile, self-interactions will heat and expand the core, thereby reducing the central density. At this stage, the mean free path λ of the self-interactions is longer than the Jeans length H. At intermediate times, the halo density decreases and remains cored. After a minimum density is reached and the core becomes isothermal, collapse begins slowly. For longer evolution times, it eventually collapses. For a cross section of $\sigma_m \sim 0.1\text{-}10\ \mathrm{cm^2\,g^{-1}}$, the halo keeps a cored profile for a substantial amount of time, while larger cross sections accelerate the collapse [2].

3 Gravothermal Conductive Fluid Model

The gravothermal conductive fluid approximation model describes a virially static, spherically symmetric, gravitating fluid that can transport heat via particle collisions. It employs four fundamental equations: conservation of mass, hydrostatic equilibrium, heat conduction, and the laws of thermodynamics. The following section briefly outlines the derivation of these equations as presented by Pollack [4].

3.1 Conservation of Mass

The equation of conservation of mass of a spherical symmetric density distribution $\rho(r)$ is

$$M(r) = 4\pi \int_0^r r'^2 \rho(r') \mathrm{d}r', \tag{2}$$

which results in the differential equation

$$\frac{\mathrm{d}M}{\mathrm{d}r} = 4\pi r^2 \rho. \tag{3}$$

In this definition, $M(r)$ is the enclosed mass at radius r.

3.2 Hydrostatic Equilibrium

Hydrostatic Equilibrium describes the balance between outward pressure and the inward acting force of gravity. Starting from the Poisson Equation for the gravitational potential ϕ

$$\nabla^2 \phi = 4\pi G \rho, \tag{4}$$

which is simplified by implying a spherically symmetric potential $\phi(r)$

$$\frac{1}{r^2} \frac{\partial}{\partial r} \left(r^2 \frac{\partial \phi}{\partial r} \right) = 4\pi G \rho, \tag{5}$$

and by using (3), we get:

$$\frac{\partial \phi}{\partial r} = \frac{GM}{r^2}. \tag{6}$$

Then, by looking at Euler's equation

$$\frac{\partial \vec{v}}{\partial t} + \left(\vec{v} \cdot \vec{\nabla}\right) \vec{v} = -\frac{1}{\rho}\vec{\nabla}P - \vec{\nabla}\phi, \tag{7}$$

and knowing that for a fluid in hydrostatic equilibrium $\vec{v} = 0$, we can see that pressure is balanced by gravity:

$$\vec{\nabla}P = -\vec{\nabla}\phi \tag{8}$$

$$\frac{\partial P}{\partial r} = -\rho\frac{GM}{r^2} \tag{9}$$

3.3 Heat Flux

The Fourier equation describes that the heat flux $\vec{q}$ is proportional to the negative temperature gradient $-\vec{\nabla} \cdot T$, with the thermal conductivity κ as the proportionality constant.

$$\vec{q} = -\kappa\vec{\nabla}T \tag{10}$$

Because the system is spherically symmetric, the heat flux only has a radial component $\vec{q} = (q_r, 0, 0)$

$$q_r = -\kappa\frac{\partial T}{\partial r} \tag{11}$$

From the heat flux, the luminosity L can be defined as the total heat conducted through a sphere at radius r:

$$\frac{L}{4\pi r^2} = q_r = -\kappa\frac{\partial T}{\partial r} \tag{12}$$

3.4 Thermodynamics

3.4.1 Equation of State

The equation of state of an ideal fluid is $P = nk_{\mathrm{B}}T$, where $n = \rho/m$ is the number density and m the mass of a particle, k_{B} the Boltzmann constant, and T the temperature. The temperature is related to the velocity $\vec{v}$ via the kinetic energy

$$\frac{3}{2}k_{\mathrm{B}}T = \frac{1}{2}m\langle\vec{v}^2\rangle, \tag{13}$$

which in turn is related to the velocity dispersion ν by assuming isotropy

$$\nu^2 \equiv \langle v_x^2\rangle = \langle v_y^2\rangle = \langle v_z^2\rangle = \frac{1}{3}\langle\vec{v}^2\rangle = \frac{k_{\mathrm{B}}T}{m}, \tag{14}$$

so the equation of state can be written as

$$P = \rho\nu^2. \tag{15}$$

For a monoatomic gas the specific internal energy per particle is

$$u = \frac{3k_{\mathrm{B}}T}{2m} = \frac{3P}{2\rho}. \tag{16}$$

3.4.2 First Law

Starting from energy conservation

$$\mathrm{d}U = T\mathrm{d}S - \rho\mathrm{d}V, \tag{17}$$

we can rewrite this into the specific quantity form

$$\mathrm{d}u = T\mathrm{d}s + \frac{P}{\rho^2}\mathrm{d}\rho, \tag{18}$$

by using

$$u = \frac{U}{m}, \quad s = \frac{S}{m}, \quad \rho = \frac{m}{V}. \tag{19}$$

Taking the specific internal energy and writing it as a function $u(P, \rho)$, the differential is

$$T\mathrm{d}s = \left.\frac{\partial u}{\partial P}\right|_{\rho} \mathrm{d}P + \left.\frac{\partial u}{\partial \rho}\right|_{P} \mathrm{d}\rho - \frac{P}{\rho^2}\mathrm{d}\rho, \tag{20}$$

which becomes

$$\mathrm{d}s = \frac{k_\mathrm{B}}{m}\left[\frac{3}{2}\frac{\mathrm{d}P}{P} - \frac{5}{2}\frac{\mathrm{d}\rho}{\rho}\right]. \tag{21}$$

After integration, we get the specific entropy

$$s = \frac{k_\mathrm{B}}{m}\ln\left(\frac{P^{3/2}}{\rho^{5/2}}\right) = \frac{k_\mathrm{B}}{m}\ln\left(\frac{\nu^3}{\rho}\right) \tag{22}$$

3.4.3 Second Law

Employing the second law of thermodynamics and assuming vanishing dissipative entropy production, such that the entropy change is given by

$$T\mathrm{d}S = \delta Q \tag{23}$$

The conservation law of the heat flux is given as the integral over the flux $\vec{q}$ through the surface $\mathrm{d}\vec{A}$

$$\dot{Q} = -\oint_{\partial V} \vec{q}\cdot\mathrm{d}\vec{A}, \tag{24}$$

and by using Gauss's theorem

$$\dot{Q} = -\int_V \vec{\nabla}\cdot\vec{q}\,\mathrm{d}V \tag{25}$$

By switching to specific quantities again, the second law becomes

$$T\left.\frac{\mathrm{d}s}{\mathrm{d}t}\right|_M = \left.\frac{1}{m}\frac{\mathrm{d}Q}{\mathrm{d}t}\right|_M = -\frac{1}{\rho}\vec{\nabla}\cdot\vec{q}. \tag{26}$$

This results in the final equation

$$\frac{\mathrm{d}}{\mathrm{d}t}\ln\left(\frac{\nu^3}{\rho}\right) = -\frac{1}{\nu^2}\frac{\mathrm{d}L}{\mathrm{d}M}, \tag{27}$$

which encodes the local conservation of energy in the system.

3.5 Thermal Conductivity

The equations derived so far describe a spherically symmetric, self-gravitating fluid in which energy is transported by heat conduction. The efficiency of this transport is governed by the thermal conductivity κ, which encodes the microscopic interaction properties. In the case of self-interacting dark matter, the interactions are elastic, hard-sphere collisions. Heat transport can be modeled using transport theory, with particles crossing a spherical surface at radius r carrying thermal energy. The resulting heat flux $q(r)$ depends on the difference between the energies transported by particles moving outward and inward across this surface with particle flux $\pm\frac{n\lambda}{\tau}$.

$$q(r) = \frac{1}{2}\left(q_+ + q_-\right) = \frac{1}{2}\left[-\frac{n\lambda}{\tau}\frac{3}{2}k_{\mathrm{B}}T_+ + \frac{n\lambda}{\tau}\frac{3}{2}k_{\mathrm{B}}T_-\right] \tag{28}$$

Using the mean free path λ and collision time τ. Assuming local equipartition of energy and applying a first-order Chapman-Enskog expansion, the temperatures associated with particles on either side of the surface can be approximated as

$$T_\pm = T(r) \pm b\lambda\frac{\partial T}{\partial r}, \tag{29}$$

where $b = \frac{25\sqrt{\pi}}{32}$ [18] is an effective impact parameter for hard sphere scattering. This results in the expression

$$\kappa = \frac{3}{2}\frac{k_{\mathrm{B}}}{m}\frac{b\rho\lambda^2}{\tau}. \tag{30}$$

The SIDM fluid properties depend on the mean free path λ and the local gravitational scale height, or the Jeans length H:

$$H = \sqrt{\frac{\nu^2}{4\pi G\rho}}. \tag{31}$$

In the SMFP regime, where $\lambda \ll H$, collisions occur frequently, which means the collision time is given by the velocity dispersion $\tau = \lambda/\nu$, which leads to

$$\kappa = 3\frac{k_{\mathrm{B}}}{m}b\rho\nu\lambda. \tag{32}$$

In the LMFP regime, $\lambda \gg H$, collisions are rare and the effective mean free path is limited by the scale height, $\lambda \to H$, and the collision time is replaced by the relaxation time t_r. The thermal conductivity then becomes

$$\kappa = \frac{3}{2}\frac{k_{\mathrm{B}}}{m}\frac{b\rho H^2}{t_r}. \tag{33}$$

Since realistic SIDM halos generally contain regions belonging to both limits, the SMFP and LMFP regimes are interpolated via

$$\kappa^{-1} = \kappa_{\mathrm{SMFP}}^{-1} + \kappa_{\mathrm{LMFP}}^{-1}, \tag{34}$$

which leads to the interpolated luminosity

$$\kappa = 3\frac{k_{\mathrm{B}}}{m}b\rho\nu^2\left[\frac{1}{\lambda} + \frac{b\nu t_r}{C\,H^2}\right]^{-1}. \tag{35}$$

The dimensionless parameter C controls the relative importance of the LMFP contribution. It is determined by comparing with N-body simulations $C \approx 0.753$ [18]. The mean free path is related to σ_m by

$$\lambda = \frac{1}{\rho\,\sigma_m}, \tag{36}$$

while the relaxation time for hard-sphere scattering is given by

$$t_r = \frac{1}{a\rho\sigma_m\nu} \tag{37}$$

with $a = \sqrt{16/\pi}$ [4].

3.6 Summary

We now have the four equations needed to explain a gravothermal fluid. By introducing a small cross-section and the SMFP and LMFP regimes, we construct a thermal conductivity κ to model a SIDM halo.

$$\frac{\mathrm{d}M}{\mathrm{d}r} = 4\pi r^2\rho \tag{38}$$

$$\frac{\mathrm{d}P}{\mathrm{d}r} = -\rho\frac{GM}{r^2} \tag{39}$$

$$\frac{L}{4\pi r^2} = q_r = -\kappa\frac{\partial T}{\partial r} \tag{40}$$

$$\frac{\mathrm{d}}{\mathrm{d}t}\ln\left(\frac{\nu^3}{\rho}\right) = -\frac{1}{\nu^2}\frac{\mathrm{d}L}{\mathrm{d}M} \tag{41}$$

Next, we will go into detail on how to find equivalent relativistic expressions, starting with an introduction to general relativity.

4 General Relativity

4.1 Introduction to GR

In the Newtonian descriptions of the collapse of SIDM halos, gravity is implemented as a force acting on particles. In General Relativity, gravity is no longer interpreted as a force but as a consequence of the curvature of space-time. We introduce the basic relations needed to construct the theory of general relativity, following the descriptions in the textbook from Rezzolla and Zanotti [19]. Space-time is a four-dimensional pseudo-Riemannian manifold composed of three spatial dimensions and one time dimension. It is non-Euclidean where distances s between events can be measured using the metric tensor $\boldsymbol{g}$:

$$\mathrm{d}s^2 = g_{\mu\nu}\mathrm{d}x^\mu \mathrm{d}x^\nu. \tag{42}$$

For flat-space, i.e., Minkowski-space, the metric tensor is $g_{\mu\nu} = \mathrm{diag}(-1, 1, 1, 1)$ with the line element

$$\mathrm{d}s^2 = -c^2\mathrm{d}t^2 + \mathrm{d}x^2 + \mathrm{d}y^2 + \mathrm{d}z^2. \tag{43}$$

There are two possible conventions for the signs of the metric tensor; in this work, the mostly-positive convention, denoted $(-,+,+,+)$, is adopted. The distance between two points on a pseudo-Riemannian manifold can be positive, negative, or zero. Using the mostly positive convention $(-,+,+,+)$, distances greater than zero $\mathrm{d}s > 0$ are called space-like, those less than zero $\mathrm{d}s < 0$ are time-like, and those equal to zero $\mathrm{d}s = 0$ are null-like. Only time-like and null-like events are causally connected. In addition to the manifold, a connection Γ must be defined to differentiate between tangent vector fields. The ordinary derivative cannot be used because the derivative of a vector does not transform as a tensor. Therefore, the covariant derivative ∇ is introduced to ensure proper transformation properties.

$$\nabla_\mu V^\alpha = \partial_\mu V^\alpha + \Gamma^\alpha_{\mu\nu} V^\nu \tag{44}$$

The connection Γ is called the Christoffel symbol and doesn't transform like a tensor. By specifying that the covariant derivative should be a Levi-Civita connection, it has to be compatible with the metric $\nabla \boldsymbol{g} = 0$, i.e., parallel transport of vectors must conserve lengths, and it has to be torsion-free $\Gamma^\alpha_{[\mu\nu]} = 0$. The Christoffel symbols are computed by

$$\Gamma^\alpha_{\mu\nu} = \frac{1}{2} g^{\alpha\beta} \left(\partial_\mu g_{\nu\beta} + \partial_\nu g_{\mu\beta} - \partial_\beta g_{\mu\nu}.\right) \tag{45}$$

Now we have the tools to measure a manifold's intrinsic curvature. The intrinsic curvature is the curvature that exists within the hypersurface itself and is not from the context of a higher dimension in which the surface could be embedded. It is described by the Riemann tensor $\boldsymbol{R}$, which measures the difference in commutation $\boldsymbol{V}$ along two directions ∂_μ and ∂_ν.

$$\nabla_{[\mu}\nabla_{\nu]} V^\alpha = R^\alpha{}_{\mu\nu\lambda} V^\lambda. \tag{46}$$

By contracting the rank 4 Riemann tensor, we get the rank 2 Ricci tensor $R_{\mu\nu} = R^\alpha{}_{\mu\alpha\nu}$, with the Ricci scalar $R = R_\mu{}^\mu$ as its trace. The Einstein tensor $\boldsymbol{G}$ is built from the Ricci

tensor and scalar. It encodes the curvature of the spacetime and has zero divergence $\nabla_\mu G^{\mu\nu} = 0$ by definition.

$$G_{\mu\nu} = R_{\mu\nu} + \frac{1}{2} g_{\mu\nu} R \tag{47}$$

The Einstein Equations then describe gravity as a result of the intrinsic curvature of spacetime, generated by mass and energy, by relating the Einstein Tensor to an energy-momentum source term, the Energy-Momentum tensor $\boldsymbol{T}$.

$$8\pi T_{\mu\nu} = R_{\mu\nu} - \frac{1}{2} g_{\mu\nu} R \tag{48}$$

4.2 Tolman-Oppenheimer-Volkoff equations

The Einstein equations consist of 10 equations in total, due to the symmetry of $\boldsymbol{G}$. However, four of these are not independent because the divergence of $\boldsymbol{G}$ vanishes, so only 6 independent equations remain. By assuming a static, spherically symmetric system, the system of equations can be further reduced. The generic line element with these properties is

$$\mathrm{d}s^2 = -c^2 \mathrm{e}^{2\Phi(r)} \mathrm{d}t^2 + \mathrm{e}^{2\lambda(r)} \mathrm{d}r^2 + r^2 \mathrm{d}\Omega^2, \tag{49}$$

where $\lambda(r)$ and $\phi(r)$ are generic functions of coordinate radius r. Using this and the Einstein Field equation

$$8\pi T_{\mu\nu} = R_{\mu\nu} - \frac{1}{2} g_{\mu\nu} R, \tag{50}$$

with the energy-momentum Tensor $\boldsymbol{T}$ of an ideal fluid

$$T_{\mu\nu} = \frac{1}{c^2}(e + P) u_\mu u_\nu + P g_{\mu\nu} \tag{51}$$

$$T_\mu{}^\nu = \begin{pmatrix} -e & 0 & 0 & 0 \\ 0 & P & 0 & 0 \\ 0 & 0 & P & 0 \\ 0 & 0 & 0 & P \end{pmatrix} \tag{52}$$

and the energy-momentum-conservation equation

$$\nabla \boldsymbol{T} = 0, \tag{53}$$

the TOV equations [7, 8] can be derived

$$\frac{\partial M}{\partial r} = 4\pi r^2 \rho, \tag{54}$$

$$\frac{\partial \Phi}{\partial r} = \frac{G}{c^2} \frac{M c^2 + 4\pi r^3 P}{r\,(r c^2 - 2GM)} = \frac{GM}{r^2 c^2} \left(1 + \frac{4\pi r^3 P}{M c^2}\right) \left(1 - \frac{2GM}{r c^2}\right)^{-1}, \tag{55}$$

$$\frac{\partial P}{\partial r} = -\left(\rho c^2 + P\right) \frac{\partial \Phi}{\partial r} = -\rho \frac{GM}{r^2} \left(1 + \frac{P}{\rho c^2}\right) \left(1 + \frac{4\pi r^3 P}{M c^2}\right) \left(1 - \frac{2GM}{r c^2}\right)^{-1}, \tag{56}$$

with

$$e = \rho c^2, \tag{57}$$

$$\mathrm{e}^{2\lambda(r)} = \left(1 - \frac{2GM(r)}{rc^2}\right)^{-1}. \tag{58}$$

In these equations, $M(r)$ describes the enclosed 'gravitational' mass at radius r, $P(r)$ is the pressure, $e(r)$ is the energy density, and $\rho(r) = e/c^2$ is the energy density expressed in units of mass per volume. The dimensionless variable $\phi(r)$ times c^2 reduces to the Newtonian gravitational potential $\phi'_{\mathrm{Newt}} = \frac{GM}{r^2}$ in the limit $c \to \infty$. Therefore, it will be referred to colloquially as the 'gravitational potential'. The TOV equations describe the hydrostatic equilibrium of a spherically symmetric, static, ideal fluid.

4.2.1 Equation of State

To evaluate the TOV equations, we need to introduce an equation of state (EOS). We assume a perfect, relativistic, nearly collisionless (ideal) fluid with particles that move isotropically in each fluid element with a root-mean-square velocity $v_{\mathrm{rms}} \equiv \langle v^2 \rangle$. In an isotropic velocity distribution, the velocity dispersion ν is defined as $\nu^2 \equiv \langle v_i^2 \rangle = v_{\mathrm{rms}}^2/3$. A relativistic ideal gas still follows the ideal gas law $P = nk_{\mathrm{B}}T$, as derived by F. Jüttner [20]. For the most part, I follow the logic from Shapiro [9]. There the EOS is $P = nk_{\mathrm{B}}T = \rho\nu^2$ and $\rho = \gamma\rho_0$, $\rho_0 = mn$, with the Lorentz factor

$$\gamma = \frac{1}{\sqrt{1 - \langle v^2 \rangle / c^2}} = \frac{1}{\sqrt{1 - 3\nu^2/c^2}}, \tag{59}$$

where ρ_0 is the rest-mass density and m the particle mass. This results in $k_{\mathrm{B}}T = \gamma m \nu^2$.

4.3 Conservation of Rest Mass

In the Newtonian gravothermal fluid description, the enclosed mass is typically used as a Lagrangian variable to label a given mass shell, whose radial position r and associated quantities, such as pressure and density, evolve over time. The cumulative gravitational mass M is not an appropriate Lagrangian variable, since it includes energy contributions and therefore does not remain constant during the evolution. To obtain the proper analogue to the Newtonian formulation, the enclosed rest mass M_0 is used. It's derived from the volume integral over the rest-mass density ρ_0. First, we need to find the induced 3-metric $\gamma_{ij}^{(3)}$ for constant time. The line element of this induced metric is

$$\mathrm{d}l^2 = \mathrm{e}^{2\lambda}\,\mathrm{d}r^2 + r^2\,\mathrm{d}\theta + r^2\sin^2\theta\,\mathrm{d}\phi, \tag{60}$$

with

$$\gamma_{ij}^{(3)} = \mathrm{diag}\left(\mathrm{e}^{2\lambda}, r^2, r^2\sin^2\theta\right), \tag{61}$$

and the determinant

$$\gamma^{(3)} = \det\left(\gamma_{ij}^{(3)}\right) = \mathrm{e}^{2\lambda} r^4 \sin^2\theta. \tag{62}$$

Thus, the proper volume element is

$$\mathrm{d}V = \sqrt{\gamma^{(3)}}\,\mathrm{d}r\,\mathrm{d}\theta\,\mathrm{d}\phi = \mathrm{e}^{\lambda} r^2 \sin\theta\,\mathrm{d}r\,\mathrm{d}\theta\,\mathrm{d}\phi, \tag{63}$$

and the resulting rest mass integral and differential

$$M_0(r) = \int_V \rho_0 \,\mathrm{d}V = 4\pi \int_0^r \rho_0(r') r'^2 \mathrm{e}^{\lambda(r')} \,\mathrm{d}r' \tag{64}$$

$$\Rightarrow \frac{\mathrm{d}M_0}{\mathrm{d}r} = 4\pi r^2 \mathrm{e}^{\lambda} \rho_0 \tag{65}$$

4.4 Heat Flux

Fourier's law of heat conduction states that the thermal flux $\vec{q}$ is proportional to the negative gradient of temperature T times heat conductivity κ

$$\vec{q} = -\kappa \vec{\nabla} T. \tag{66}$$

It must be mentioned that, unlike in classical flat space-time, the temperature is not constant in curved space-time in thermal equilibrium. Instead, the value $\sqrt{-g_{tt}}\, T = \text{const}$ is conserved, this is known as the Ehrenfest-Tolman effect [21]. A similar relation can be made for the heat-flux $\sqrt{-g_{tt}}\, q = \text{const}$, leading to the expression for radial heat flux

$$q_r = -\frac{\kappa}{\mathrm{e}^{\phi}} \frac{\partial \left(T \mathrm{e}^{\phi}\right)}{\partial r}, \tag{67}$$

as derived by Ram [22].

Local Luminosity $L_{\text{local}}(r)$ is the total heat flux through the surface $n_\mu \mathrm{d}A$ with the normal n_μ, which encloses the volume V at radius r. The normal n_μ of the hypersurface $r, t = \text{const}$ is proportional to the radial one-form

$$n_\mu \propto \partial_\mu r = (0, 1, 0, 0). \tag{68}$$

Because $\boldsymbol{n}$ is space-like, the normalization condition is $n_\mu n^\mu = 1$, this results in

$$n_\mu = (0, \alpha, 0, 0) \;\text{ and }\; n^\mu = (0, \alpha^{-1}, 0, 0), \tag{69}$$

with $\alpha = \sqrt{g_{rr}} = \mathrm{e}^{\lambda}$. The proper area element $\mathrm{d}A$ is derived by taking the determinant of the induced 2-metric $\gamma^{(2)}$ of the 2-sphere $\mathrm{d}l^2 = r^2 \,\mathrm{d}\theta^2 + r^2 \sin^2\theta \,\mathrm{d}\phi^2$

$$\gamma^{(2)} = \det\left(\mathrm{diag}(r^2, r^2 \sin^2\theta)\right) = r^4 \sin^2\theta, \quad \mathrm{d}A = \sqrt{\gamma^{(2)}}\,\mathrm{d}\theta\,\mathrm{d}\phi. \tag{70}$$

Thus, the local luminosity is

$$L_{\text{local}} = \int_{\partial V} q_\mu n^\mu \mathrm{d}A = 4\pi r^2 q_r \mathrm{e}^{-\lambda}. \tag{71}$$

Luminosity is just the energy rate over time

$$L_{\text{local}} = \frac{\mathrm{d}E_{\text{local}}}{\mathrm{d}\tau}, \tag{72}$$

to get a Luminosity as measured by a distant observer L we need to account for the fact that the local energy and proper time are gravitationally redshifted by a factor of $\sqrt{g_{tt}} = \mathrm{e}^{\phi}$ and $\sqrt{g^{tt}} = \mathrm{e}^{-\phi}$ respectively [19]:

$$L = \frac{\mathrm{d}E}{\mathrm{d}t} = \frac{\mathrm{e}^{\phi}\,\mathrm{d}E_{\text{local}}}{\mathrm{e}^{-\phi}\,\mathrm{d}\tau} = \mathrm{e}^{2\phi} L_{\text{local}} = 4\pi r^2 q_r \mathrm{e}^{2\phi - \lambda}. \tag{73}$$

4.5 Conservation of Energy

The TOV equations describe a static system without heat flux. In order to get equivalent equations for the thermodynamic statements, we need to introduce q into the energy-momentum tensor. Because our system is spherically symmetric, heat-flux only has a radial component $q_\mu = (0, q_r, 0, 0)$ and is orthogonal to the fluid four-velocity $u_\mu = (u_t, 0, 0, 0)$. This results in modifications to the spatial components of the energy flux $T^{i,0}$ and the momentum density $T^{0,i}$ of the energy-momentum tensor [19].

$$T^{\mu\nu} = \frac{1}{c^2}\left(e + P\right) u^\mu u^\nu + P g^{\mu\nu} + \frac{1}{c^2}\left(q^\mu u^\nu + q^\nu u^\mu\right) \tag{74}$$

$$T_\mu{}^\nu = \begin{pmatrix} -e & -q^r/c & 0 & 0 \\ q_r/c & P & 0 & 0 \\ 0 & 0 & P & 0 \\ 0 & 0 & 0 & P \end{pmatrix}. \tag{75}$$

The General Relativistic equivalent of the Euler Equations is:

$$\nabla_\mu T^{\mu\nu} = 0 \tag{76}$$

To get separate equations for energy and momentum, we can break the covariant derivative of $\boldsymbol{T}$ apart into a parallel and an orthogonal component to $\boldsymbol{u}$, which need to be zero individually. For this, we need to define the projection tensor $\boldsymbol{h}$ as $h^{\mu\nu} = g^{\mu\nu} + \frac{1}{c^2} u^\mu u^\nu$, which fulfills $\boldsymbol{h} \cdot \boldsymbol{u} = 0$.

$$u_\nu \nabla_\mu T^{\mu\nu} = -u^\mu \nabla_\mu e + \frac{e + P}{n} u^\mu \nabla_\mu n - \nabla_\mu q^\mu + \frac{1}{c^2} a_\mu q^\mu = 0 \tag{77}$$

$$h^\sigma{}_\nu \nabla_\mu T^{\mu\nu} = h^{\sigma\mu} \nabla_\mu P + \frac{1}{c^2}(e + P) a^\sigma + \frac{1}{c^2}\left[q^\sigma \nabla_\mu u^\mu + q^\mu \nabla_\mu u^\sigma + u^\mu \nabla_\mu q^\sigma - \frac{1}{c^2} u^\sigma a_\mu q^\mu\right] = 0 \tag{78}$$

The equation (77) describes energy conservation, and equation (78) describes the conservation of momentum. In deriving this form, the continuity equation $\nabla_\mu (n u^\mu) = 0$, with the number density n was used to write $\nabla_\mu u^\mu = -(u^\mu \nabla_\mu n)/n$. Furthermore, the four acceleration is defined as the parallel transport of $\boldsymbol{u}$ along itself $a^\nu \equiv u^\mu \nabla_\mu u^\nu$. By using $g_{\mu\nu} u^\mu u^\nu = -c^2$ and (45) to calculate $\Gamma^0_{\mu 0} = \partial_\mu \phi$, we get $a_\mu = c^2 \partial_\mu \phi$. The directional derivative $u^\mu \nabla_\mu (\,\cdot\,)$ is just the derivative towards the proper time $\partial_\tau (\,\cdot\,)$. Therefore, the equation for the conservation of energy is

$$\frac{\mathrm{d}e}{\mathrm{d}\tau} - \frac{e + P}{n} \frac{\mathrm{d}n}{\mathrm{d}\tau} = -\nabla_\mu q^\mu - q^r \frac{\mathrm{d}\phi}{\mathrm{d}r}. \tag{79}$$

Now we can apply the EOS to the energy equation (79). The left-hand side results in:

$$\begin{aligned}
\frac{\mathrm{d}e}{\mathrm{d}\tau} - \frac{e+P}{n}\frac{\mathrm{d}n}{\mathrm{d}\tau} &= e\frac{\mathrm{d}\ln e}{\mathrm{d}\tau} - (e+P)\frac{\mathrm{d}\ln n}{\mathrm{d}\tau} \\
&= e\frac{\mathrm{d}\ln e/n}{\mathrm{d}\tau} - P\frac{\mathrm{d}\ln n}{\mathrm{d}\tau} \\
&= P\left(\frac{c^2}{\nu^2}\frac{\mathrm{d}\ln\gamma}{\mathrm{d}\tau} - \frac{\mathrm{d}\ln n}{\mathrm{d}\tau}\right) \\
&= P\left(\frac{\mathrm{d}\ln\gamma^3\nu^3/c^3}{\mathrm{d}\tau} - \frac{\mathrm{d}\ln n}{\mathrm{d}\tau}\right) \\
&= P\frac{\mathrm{d}}{\mathrm{d}\tau}\ln\left(\frac{\gamma^3\nu^3}{n\,c^3}\right) \\
&= \rho_0 T\frac{\mathrm{d}s}{\mathrm{d}\tau}
\end{aligned} \tag{80}$$

$$\frac{\mathrm{d}e}{\mathrm{d}\tau} - \frac{e+P}{n}\frac{\mathrm{d}n}{\mathrm{d}\tau} = P\frac{\mathrm{d}}{\mathrm{d}\tau}\ln\left(\frac{\gamma^3\nu^3}{n\,c^3}\right) = \rho_0 T\frac{\mathrm{d}s}{\mathrm{d}\tau} \tag{81}$$

This is just the first law of thermodynamics with the specific entropy $s = \frac{k_\mathrm{B}}{m}\ln\left(\frac{\gamma^3\nu^3}{n\,c^3}\right)$. The right-hand side becomes:

$$\begin{aligned}
-\nabla_\mu q^\mu - \frac{1}{c^2}a_\mu q^\mu &= -\frac{\mathrm{d}q^r}{\mathrm{d}r} - q^r\Gamma^\mu_{\mu r} - \frac{1}{c^2}a_r q^r \\
&= -\frac{\mathrm{d}q^r}{\mathrm{d}r} - q^r\left[\frac{2}{r} + \frac{\mathrm{d}\phi}{\mathrm{d}r} + \frac{\mathrm{d}\lambda}{\mathrm{d}r}\right] - q^r\frac{\mathrm{d}\phi}{\mathrm{d}r} \\
&= -\frac{\mathrm{d}q^r}{\mathrm{d}r} - q^r\left[\frac{2}{r} + 2\frac{\mathrm{d}\phi}{\mathrm{d}r} + \frac{\mathrm{d}\lambda}{\mathrm{d}r}\right] \\
&= -\frac{\mathrm{d}q^r}{\mathrm{d}r} - q^r\frac{\mathrm{d}\ln r^2\mathrm{e}^{2\phi+\lambda}}{\mathrm{d}r} \\
&= -\frac{1}{r^2\mathrm{e}^{2\phi+\lambda}}\left[r^2\mathrm{e}^{2\phi+\lambda}\frac{\mathrm{d}q^r}{\mathrm{d}r} + q^r\frac{\mathrm{d}r^2\mathrm{e}^{2\phi+\lambda}}{\mathrm{d}r}\right] \\
&= -\frac{1}{r^2\mathrm{e}^{2\phi+\lambda}}\frac{\mathrm{d}}{\mathrm{d}r}\left[q^r r^2\mathrm{e}^{2\phi+\lambda}\right] \\
&= -\frac{1}{r^2\mathrm{e}^{2\phi+\lambda}}\frac{\mathrm{d}}{\mathrm{d}r}\left[q_r r^2\mathrm{e}^{2\phi-\lambda}\right] \\
&= -\frac{1}{4\pi r^2\mathrm{e}^{2\phi+\lambda}}\frac{\mathrm{d}L}{\mathrm{d}r} \\
&= -\frac{\rho_0}{\mathrm{e}^{2\phi}}\frac{\mathrm{d}L}{\mathrm{d}M_0}
\end{aligned} \tag{82}$$

The approximation $\partial_\tau \approx \mathrm{e}^{-\phi}\partial_t$, "since the mean fluid velocity is everywhere negligible in a virialized, spherical, quasistatic system" [9, p. 13]. So, we obtain a final expression for the conservation of energy in the general-relativistic conductive-fluid approximation:

$$\frac{\mathrm{d}}{\mathrm{d}t}\ln\left(\frac{\gamma^3\nu^3}{\rho_0}\right) = -\frac{1}{\gamma\nu^2\mathrm{e}^{\phi}}\frac{\mathrm{d}L}{\mathrm{d}M_0}. \tag{83}$$

4.6 Heat Conduction Step

During a heat-conduction step, the rest-mass density ρ_0 is kept constant. It is an isochoric process that satisfies the energy conservation equation (83). We define the specific internal energy

$$u \equiv \frac{3k_\mathrm{B}T}{2m} = \frac{3P}{2\rho_0} = \frac{3}{2}\gamma\nu^2 \tag{84}$$

and find an expression for γ in terms of u by writing (59) as

$$\gamma^{-2} = 1 - 2\frac{u}{c^2}\gamma^{-1}, \tag{85}$$

then solving the quadratic equation and demanding that $\gamma \geq 1$, $\forall u \geq 0$, we get

$$\gamma(u) = \frac{u}{c^2} + \sqrt{\left(\frac{u}{c^2}\right)^2 + 1}. \tag{86}$$

This allows us to express the left-hand side of the energy conservation equation while keeping ρ_0 constant. First we need to find the derivative of γ expressed as a derivative of u:

$$\frac{\mathrm{d}\ln\gamma}{\mathrm{d}t} = \frac{\gamma^2-1}{\gamma^2+1}\frac{\mathrm{d}\ln u}{\mathrm{d}t}$$

Then we rewrite the left-hand side of equation (83):

$$\begin{aligned}
\frac{\mathrm{d}}{\mathrm{d}t}\ln\left(\frac{\gamma^3 u^{3/2}}{\rho_0}\right)\bigg|_{\rho_0} &= \frac{\mathrm{d}}{\mathrm{d}t}\ln\left(\frac{\gamma^{3/2} u^{3/2}}{\rho_0}\right)\bigg|_{\rho_0} \\
&= \frac{3}{2}\left(\frac{\mathrm{d}\ln\gamma}{\mathrm{d}t}\bigg|_{\rho_0} + \frac{\mathrm{d}\ln u}{\mathrm{d}t}\bigg|_{\rho_0}\right) \\
&= \frac{3}{2}\left(\frac{\gamma^2-1}{\gamma^2+1}\,\frac{\mathrm{d}\ln u}{\mathrm{d}t}\bigg|_{\rho_0} + \frac{\mathrm{d}\ln u}{\mathrm{d}t}\bigg|_{\rho_0}\right) \\
&= \frac{3\gamma^2}{\gamma^2+1}\cdot\frac{1}{u}\,\frac{\mathrm{d}u}{\mathrm{d}t}\bigg|_{\rho_0}
\end{aligned}$$

By combining this with the right-hand side of equation (83), we get a description of how u changes over time:

$$\frac{\mathrm{d}}{\mathrm{d}t}\ln\left(\frac{\gamma^3 u^{3/2}}{\rho_0}\right)\bigg|_{\rho_0} = -\frac{1}{\gamma\nu^2\mathrm{e}^{\phi}}\frac{\mathrm{d}L}{\mathrm{d}M_0}$$

$$\Rightarrow \quad \frac{\mathrm{d}u}{\mathrm{d}t}\bigg|_{\rho_0} = -\frac{1+1/\gamma^2}{2\mathrm{e}^{\phi}}\frac{\mathrm{d}L}{\mathrm{d}M_0} \tag{87}$$

The change of P over time is derived directly from u:

$$\frac{\mathrm{d}\ln P}{\mathrm{d}t}\bigg|_{\rho_0} = \frac{\mathrm{d}\ln u}{\mathrm{d}t}\bigg|_{\rho_0} \tag{88}$$

$$\frac{\mathrm{d}P}{\mathrm{d}t}\bigg|_{\rho_0} = \frac{P}{u}\,\frac{\mathrm{d}u}{\mathrm{d}t}\bigg|_{\rho_0} \tag{89}$$

Comparing this to the Newtonian result:

$$\frac{\mathrm{d}u}{\mathrm{d}t} = -\frac{\mathrm{d}L}{\mathrm{d}M} \tag{90}$$

$$\frac{\mathrm{d}P}{\mathrm{d}t} = \frac{P}{u}\frac{\mathrm{d}u}{\mathrm{d}t} \tag{91}$$

It is evident that the derived general relativistic results converge to the Newtonian case in the limit $c \to \infty$.

4.7 Summary

The resulting equations are:

$$\frac{\partial M}{\partial r} = 4\pi r^2 \rho \tag{92}$$

$$\frac{\partial \Phi}{\partial r} = \frac{G}{c^2}\frac{Mc^2 + 4\pi r^3 P}{r\left(rc^2 - 2GM\right)} \tag{93}$$

$$\frac{\partial P}{\partial r} = -\rho\frac{GM}{r^2}\left(1 + \frac{P}{\rho c^2}\right)\left(1 + \frac{4\pi r^3 P}{Mc^2}\right)\left(1 - \frac{2GM}{rc^2}\right)^{-1} \tag{94}$$

$$\frac{L}{4\pi r^2 \mathrm{e}^{2\phi-\lambda}} = q_r = -\frac{\kappa}{\mathrm{e}^{\phi}}\frac{\partial\left(T\mathrm{e}^{\phi}\right)}{\partial r} \tag{95}$$

$$\frac{\mathrm{d}}{\mathrm{d}t}\ln\left(\frac{\gamma^4\nu^3}{\rho}\right) = -\frac{1}{\nu^2\gamma\mathrm{e}^{\phi}}\frac{\mathrm{d}L}{\mathrm{d}M_0} \tag{96}$$

In comparison to the Newtonian case, the gravitational potential ϕ has to be evaluated, because the heat conduction explicitly depends on it. These equations are equivalent to the Newtonian expressions if we remember that $\phi \cdot c^2 \to \phi_{\mathrm{Newt}}$ for $c \to \infty$, then the limit of the exponential is $\mathrm{e}^{\phi} \to \mathrm{e}^{\phi_{\mathrm{Newt}}/c^2} \to 1$ for $c \to \infty$. For the thermal conductivity κ, the expression from subsection 3.5 is used. We can now start discussing the numerical implementation.

5 Numerical Implementation

The broad numerical implementation is outlined in Algorithm 1.

Algorithm 1: General Simulation Loop

```
Compute initial conditions;
Update variables;
t ← 0;
while t < t_max do
    Heat convection step;
    repeat
        Hydrostatic Adjustment Step;
    until Hydrostatic Equilibrium achieved;
    Update variables;
    t ← t + Δt;
```

At each timestep, it is assumed that the fluid remains in virial equilibrium, meaning the timescale for achieving hydrostatic equilibrium is much shorter than that of conductive particle interactions. The code implements this through two primary steps. When

a density and pressure profile satisfies hydrostatic equilibrium, it is perturbed via the heat-conduction equation, which governs irreversible heat flow within the system. Following each conduction step, the system departs from equilibrium and is subsequently restored through one or more hydrostatic adjustment steps. This procedure maintains virial equilibrium throughout the simulation.

A halo is modeled as a series of N concentric shells. Each shell has properties defined as averages across a shell $P, \rho_0, \rho, e, \nu, T, u, \kappa, K_{\text{eff}}$ (intensive quantities) and on the outer boundary of a shell $M_0, M, r, \phi, \lambda, L, q_r, V$ (extensive quantities). This means that the pressure P_i inside the i-th shell corresponds to a radius of $r_{i-1/2}$. When discretizing the equations, keeping track of indices and their meanings is especially important. For example, consider the discretization of the conservation of mass:

$$\frac{\mathrm{d}M}{\mathrm{d}r} = 4\pi r^2 \rho \;\Rightarrow\; \begin{cases} \frac{M_i - M_{i-1}}{r_i - r_{i-1}} = 4\pi \left(\frac{r_i + r_{i-1}}{2}\right)^2 \rho_i & \text{centered around } \rho_i \\ \frac{M_{i+1} - M_{i-1}}{r_{i+1} - r_{i-1}} = 4\pi r_i^2 \left(\frac{\rho_i + \rho_{i+1}}{2}\right) & \text{centered around } r_i \end{cases} \tag{97}$$

There are two ways to obtain it, either by centering around the center of a shell (trapezoidal rule; P, ρ, etc.) or around the boundary (midpoint rule; M, r, etc.). The code is written in Python, using libraries such as NumPy [23], SciPy [24], SymPy [25], AstroPy [26], and Numba [27]. Each shell is indexed by $i \in [0, N-1]$. In the code, not every variable-array has length N, and sometimes extended arrays are used, which shift the array by one and set the first entry to zero (a ghost cell). Python's array slicing is utilized as much as possible because it is very efficient, makes the code much more readable, and reduces boilerplate for-loops. Array slicing helps operate on arrays of different lengths. For example, if the average across the ith-shell $\bar{x}_i$ of a boundary defined variable x_i is needed, this is done:

```
import numpy as np

delta_x = np.empty_like(x)
delta_x[1:] = (x[1:]+x[:-1])/2
delta_x[0]  = x[0]/2
```

Listing 1: Array slicing example

When computing numerous finite differences, employing ghost cells at the center with a value of 0 can be advantageous. This approach enables single-step calculations, as the difference at the central index is automatically addressed.

5.1 Normalization

By choosing appropriate normalisation factors, it's possible to write the equations with dimensionless variables. A variable χ can be written as the multiplication of a dimensionless parameter $\widetilde{\chi}$ times a normalisation factor χ_N. If chosen appropriately, the individual factors in an equation will cancel each other out. The normalization factors are:

$$\begin{aligned} M_N &= 4\pi \rho_N r_N^3, \quad u_N = \frac{G M_N}{r_N}, \qquad P_N = u_N \rho_N, \\ \nu_N &= \sqrt{u_N}, \qquad t_N = \frac{1}{\sqrt{4\pi G \rho_N}}, \quad L_N = G \frac{M_N^2}{r_N t_N}, \\ \phi_N &= 1, \qquad \lambda_N = 1 \end{aligned} \tag{98}$$

Only the values of r_N and ρ_N need to be specified. These normalisations mean we can effectively replace G and 4π with 1 in our equations. By introducing a dimensionless factor

$x = u_N/c^2$, we can effectively replace any $1/c^2$ with x after switching to dimensionless variables. For example:

$$\mathrm{e}^{\lambda} = \left(1 - \frac{2GM}{rc^2}\right)^{-1/2} \quad \Rightarrow \quad \mathrm{e}^{\lambda} = \left(1 - \frac{2\tilde{M}}{\tilde{r}}x\right)^{-1/2} \tag{99}$$

$$\frac{\mathrm{d}M}{\mathrm{d}r} = 4\pi r^2\rho \quad \Rightarrow \quad \frac{\mathrm{d}\tilde{M}}{\mathrm{d}\tilde{r}} = \tilde{r}^2\tilde{\rho} \tag{100}$$

For discretized equations, dimensionless variables are used, omitting the tilde notation.

The normalization $c = 1$ is not adopted, as it is not a natural choice in the Newtonian formulation and would cause significant variation in the magnitudes of P, ρ, and M. Additionally, this approach allows the Newtonian limit to be easily identified by taking $x \to 0$ for $c \to \infty$.

5.2 Initial Conditions

At the beginning of the simulation, the rest-mass profile and density profile $\rho_0(r)$ are specified to calculate the profiles $M_0(r)$ and $P(r)$. In SIDM simulations, a model function is choosen for $\rho_0(r)$ like the Navarro-Frenk-White (NFW) profile [13]

$$\rho_{\mathrm{NFW}}(r) = \frac{\rho_s}{\frac{r}{r_s}\left(1 + \frac{r}{r_s}\right)^2}, \tag{101}$$

where r_s and ρ_s are the characteristic radius and density of the halo. The radius is initialized logarithmically from a small value $r_{\min}$ to a larger one $r_{\max}$, while avoiding the value of $r = 0$. Let's first look at how this is used to get initial data in the Newtonian regime. The conservation of mass is given by the differential

$$\frac{\mathrm{d}M_0}{\mathrm{d}r} = 4\pi r^2\rho_0 \tag{102}$$

and hydrostatic equilibrium by

$$\frac{\mathrm{d}P}{\mathrm{d}r} = -\rho_0\frac{GM_0}{r^2}. \tag{103}$$

If the profile $\rho_0(r)$ is specified by a model function like the NFW profile, then these differentials can be integrated in sequence. For some profiles, analytical solutions exist. For the NFW profile, the mass is

$$M_0(r) = 4\pi\rho_s r_s^3\int_0^{r/r_s}\frac{x}{(1+x)^2}\mathrm{d}x = 4\pi\rho_s r_s^3\left[\ln(1 + r/r_s) - \frac{r/r_s}{1 + r/r_s}\right] \tag{104}$$

Integrating the pressure is less straightforward, but still possible

$$\int_{P(r/r_s)}^{P(\infty)}\mathrm{d}P' = -4\pi\rho_s^2 r_s^2 G\int_{r/r_s}^{\infty}\frac{(1+x)\ln(1+x) - x}{x^3(1+x)^3}\mathrm{d}x, \tag{105}$$

if we assume that P vanishes at infinity $P(\infty) = 0$, switching to dimensionless variables and by using the dilogarithm Li_2 as the solution of the integral

$$\mathrm{Li}_2(x) = -\int_0^x\frac{\ln(1 - x')}{x'}\mathrm{d}x', \tag{106}$$

then the pressure is

$$P(r) = \frac{1}{2}\Big[\pi^2 - \frac{1+r(9+7r)}{r(1+r)^2} - \ln r + 6\ \mathrm{Li}_2(-r) \\ + \ln(1+r)\Big(1 - \frac{4}{r} - \frac{2}{1+r} + \frac{1}{r^2} + 3\ln(1+r)\Big)\Big]. \tag{107}$$

In the Newtonian case, this is all we need. In our case, the chosen density profile corresponds to the rest-mass density $\rho_0(r) = \rho_{\mathrm{NFW}}(r)$, which means the energy density now is a function of radius and pressure

$$\rho(r, P) = \frac{3P}{2c^2} + \sqrt{\left(\frac{3P}{2c^2}\right)^2 + \rho_0^2(r)}. \tag{108}$$

Thus, the differentials $\mathrm{d}M/\mathrm{d}r = 4\pi r^2 \rho(r, P)$ and $\mathrm{d}P/\mathrm{d}r = -\rho(r, P)\frac{GM}{r}\big(...\big)$ are coupled and cannot be solved independently. To ensure comparability between the Newtonian and general-relativistic codes, the same Lagrangian M_0 is used. The initial density ρ_0 is specified by the model function, and both the rest-mass M_0 and pressure P are calculated using the Newtonian expressions. The energy density profile is then computed from (108), and the gravitational mass profile is obtained by integrating $\mathrm{d}M/\mathrm{d}r = 4\pi r^2 \rho$.

$$\Delta M_i = \rho_i \frac{r_i^3 - r_{i-1}^3}{3} \tag{109}$$

$$M_i = \sum_{k=0}^{i} \Delta M_k \tag{110}$$

This will only satisfy the hydrostatic equilibrium from the Newtonian formulation. Therefore, a hydrostatic adjustment step is performed early to adjust the values of r, ρ, ρ_0, P, and M, while keeping the rest-mass M_0 constant.

5.3 Heat Conduction Step

The heat-conduction step is where time evolution occurs. For this, we need to write the isochoric time derivatives Δ_t of u (87) and P (89) in discrete form:

$$\Delta_t u_i = -\Delta t \frac{1 + 1/\gamma_i^2}{2\mathrm{e}^{(\phi_i + \phi_{i-1})/2}} \frac{L_i \mathrm{e}^{2\phi_i} - L_{i-1}\mathrm{e}^{2\phi_{i-1}}}{M_{0,i} - M_{0,i-1}} \tag{111}$$

$$\Delta_t P_i = P_i \frac{\Delta_t u_i}{u_i} \tag{112}$$

5.3.1 Time Difference

To get a value of Δt, there are two options. Either rewrite (87)

$$\Delta t = \min \left| u_i \frac{2\mathrm{e}^{\frac{\phi_i + \phi_{i-1}}{2}}}{1 + 1/\gamma_i^2} \frac{M_{0,i} - M_{0,i-1}}{L_i \mathrm{e}^{2\phi_i} - L_{i-1}\mathrm{e}^{2\phi_{i-1}}} \right| \tag{113}$$

or use the momentum flux

$$\Delta t = \min \left| \frac{1}{\rho_0 \nu} \right|. \tag{114}$$

5.4 Hydrostatic Equilibrium Adjustment Step

After a conduction step, the system is no longer in equilibrium. To return to equilibrium, the hydrostatic equilibrium equation needs to be relaxed numerically. The discretized TOV equation, centered around r_i is

$$\frac{P_{i+1}-P_i}{(r_{i+1}-r_{i-1})/2}+\frac{\rho_i+\rho_{i+1}+x(P_i+P_{i+1})}{2}\frac{M_i+r_i^3x(P_i+P_{i+1})/2}{r_i(r_i-2M_ix)}=0 \tag{115}$$

Depending on how close or far we are from hydrostatic equilibrium, the expression (115) will be closer or farther from zero. Hence, we want to build a residual $\mathcal{R}$ of (115), but without any denominators:

$$\begin{aligned}\mathcal{R}_i = 8\left(r_i^2-2M_ir_ix\right)(P_{i+1}-P_i)\\ +(\rho_i+\rho_{i+1}+x(P_i+P_{i+1}))(r_{i+1}-r_{i-1})\left(2M_i+r_i^3(P_i+P_{i+1})x\right).\end{aligned} \tag{116}$$

This is permitted because if expression (116) is equal to zero, then expression (115) will also be zero. When the residual is not zero, it is perturbed linearly in δr such that $\mathcal{R}_i+\delta\mathcal{R}_i=0$. Perturbative changes are denoted using δ and local differences with Δ, like $\Delta r_i=r_i-r_{i-1}$ for face-centered variables and $\Delta P_i=P_{i+1}-P_i$ for cell-centered variables. Local averages are denoted as $\bar{x}$ and are calculated as $\bar{r}_i=(r_i+r_{i-1})/2$ for face-centered and as $\bar{P}_i=(P_{i+1}+P_i)/2$ for cell-centered variables. By introducing a ghost shell in the centre of the system and extending all variables, the finite difference at the first shell is still handled correctly. This can be done because the residual is not singular at $r=0$, since we wrote it in a denominator-free form. We can therefore define the Residual $\mathcal{R}_i$ between shells 0 and $N-2$. The linear perturbation then becomes:

$$\begin{aligned}\delta\mathcal{R}_i = 16\left(r_i\delta r_i-xM_i\delta r_i-xr_i\delta M_i\right)(P_{i+1}-P_i)+8\left(r_i^2-2xM_ir_i\right)(\delta P_{i+1}-\delta P_i)\\ +(\delta\rho_i+\delta\rho_{i+1}+x(\delta P_i+\delta P_{i+1}))(r_{i+1}-r_{i-1})\left(2M_i+xr_i^3(P_i+P_{i+1})\right)\\ +(\rho_i+\rho_{i+1}+x(P_i+P_{i+1}))(\delta r_{i+1}-\delta r_{i-1})\left(2M_i+xr_i^3(P_i+P_{i+1})\right)\\ +(\rho_i+\rho_{i+1}+x(P_i+P_{i+1}))(r_{i+1}-r_{i-1})\left(2\delta M_i+3xr_i^2(P_i+P_{i+1})\delta r_i\right.\\ \left.+xr_i^3(\delta P_i+\delta P_{i+1})\right)\end{aligned} \tag{117}$$

Until now, the procedure is the same as in the Newtonian case, except that the equation for hydrostatic equilibrium is more complex in the relativistic case. The goal is to describe finding the hydrostatic equilibrium as a linear problem

$$\mathcal{R}_i+J_i{}^j\delta r_j=0, \tag{118}$$

with the elements of the matrix $\boldsymbol{J}$:

$$J_i{}^j=\frac{\partial(\delta\mathcal{R}_i)}{\partial(\delta r_j)}. \tag{119}$$

Therefore, the expressions of δP, $\delta\rho$, and δM need to be expressed in terms of δr. The rest mass density is antiproportional to a change in volume $\rho_0\propto\Delta V^{-1}$ and proportional to a change in rest mass $\rho_0\propto\Delta M_0$. Because we use M_0 as our Lagrangian variable, its perturbation is zero. This implies:

$$\frac{\delta\rho_0}{\rho_0}=\cancelto{0}{\frac{\delta\left(\Delta M_0\right)}{\Delta M_0}}-\frac{\delta\left(\Delta V\right)}{\Delta V} \tag{120}$$

Computing the volume, from the metric, involves integrating the proper volume element $\mathrm{d}V = \mathrm{e}^{\lambda} r^2 \sin\theta \,\mathrm{d}r \,\mathrm{d}\theta \,\mathrm{d}\phi$ (63):

$$V(r) = 4\pi \int_0^r r'^2 \mathrm{e}^{\lambda(r')} dr' \tag{121}$$

$$\Rightarrow \quad \frac{\mathrm{d}V}{\mathrm{d}r} = 4\pi r^2 \mathrm{e}^{\lambda(r)}. \tag{122}$$

After discretization:

$$\Delta V_i = 4\pi \frac{r_i^3 - r_{i-1}^3}{3} \left(1 - \frac{2(M_i + M_{i-1})}{r_i + r_{i-1}} x\right)^{-1/2}, \tag{123}$$

the perturbation of ΔV_i is

$$\frac{\delta(\Delta V_i)}{\Delta V_i} = \frac{x\delta\bar{M}_i}{\bar{r}_i - 2x\bar{M}_i} - \frac{\delta\bar{r}_i}{\bar{r}_i} \cdot \frac{x\bar{M}_i}{\bar{r}_i - 2x\bar{M}_i} + \frac{3r_i^2\delta r_i - 3r_{i-1}^2\delta r_{i-1}}{r_i^3 - r_{i-1}^3}. \tag{124}$$

The relaxation is characterized as an adiabatic process, i.e., no heat flow occurs, $\boldsymbol{q} = 0$. This means that the specific entropy remains constant, $\delta s = 0$. The specific entropy is derived from (81):

$$s = \frac{k_\mathrm{B}}{m} \ln \frac{\gamma^4 P^{3/2}}{\rho^{5/2} c^3} \tag{125}$$

From this, we can find a relationship between δP and $\delta\rho$.

$$\begin{aligned}
\frac{\delta s}{s} &= 4\frac{\delta\gamma}{\gamma} + \frac{3}{2}\frac{\delta P}{P} - \frac{5}{2}\frac{\delta\rho}{\rho} \\
0 &= 6\gamma^2\delta\left(\frac{P}{\rho c^2}\right) + \frac{3}{2}\frac{\delta P}{P} - \frac{5}{2}\frac{\delta\rho}{\rho} \\
0 &= 6\gamma^2\frac{P}{\rho c^2}\left(\frac{\delta P}{P} - \frac{\delta\rho}{\rho}\right) + \frac{3}{2}\frac{\delta P}{P} - \frac{5}{2}\frac{\delta\rho}{\rho} \\
0 &= \frac{3}{2}\frac{\delta P}{P}\left(1 + 4\gamma^2\nu^2/c^2\right) - \frac{3}{2}\frac{\delta\rho}{\rho}\left(\frac{5}{3} + 4\gamma^2\nu^2/c^2\right)
\end{aligned}$$

$$\Rightarrow \quad \frac{\delta P}{P} = \frac{5/3 - \nu^2/c^2}{1 + \nu^2/c^2}\frac{\delta\rho}{\rho} \tag{126}$$

$$\frac{\delta P_i}{P_i} = \frac{5/3 - x\nu_i^2}{1 + x\nu_i^2}\frac{\delta\rho_i}{\rho_i} \tag{127}$$

We recall that $\rho = \gamma\rho_0$. Therefore:

$$\begin{aligned}
\frac{\delta\rho}{\rho} &= \frac{\delta\rho_0}{\rho_0} + \frac{\delta\gamma}{\gamma} \\
\frac{\delta\rho}{\rho} &= \frac{\delta\rho_0}{\rho_0} + \frac{3}{2}\gamma^2\delta\left(\frac{P}{\rho c^2}\right) \\
\frac{\delta\rho}{\rho} &= \frac{\delta\rho_0}{\rho_0} + \frac{3}{2}\gamma^2\frac{P}{\rho c^2}\left(\frac{\delta P}{P} - \frac{\delta\rho}{\rho}\right) \\
\frac{\delta\rho_0}{\rho_0} &= \frac{\delta\rho}{\rho} - \frac{3}{2}\gamma^2\frac{P}{\rho c^2}\left(\frac{5/3 - \nu^2/c^2}{1 + \nu^2/c^2} - 1\right)\frac{\delta\rho}{\rho} \\
\left(1 + \frac{P}{\rho c^2}\right)\frac{\delta\rho_0}{\rho_0} &= \left[1 + \frac{P}{\rho c^2} - \gamma^2\frac{P}{\rho c^2}\left(1 - 3\frac{P}{\rho c^2}\right)\right]\frac{\delta\rho}{\rho}
\end{aligned}$$

$$\Rightarrow \quad \frac{\delta\rho}{\rho} = \left(1 + \frac{P}{\rho c^2}\right)\frac{\delta\rho_0}{\rho_0} \tag{128}$$

$$\frac{\delta\rho_i}{\rho_i} = \left(1 + x\frac{P_i}{\rho_i}\right)\frac{\delta\rho_{0,i}}{\rho_{0,i}} \tag{129}$$

Now we can link perturbations in pressure to density, density to rest-mass density, and rest-mass density to perturbations of r_{i-1}, r_i, and M_{i-1}, M_i. The Newtonian expressions remain unchanged, but setting $x = 0$ and recognizing that ρ and ρ_0, as well as M and M_0, describe the same quantity. In the Newtonian framework, we would use the Lagrangian grid of M, meaning that we consider all other variables relative to the enclosed mass of a shell and can use $\delta M_i = 0$. In the relativistic case, the gravitational mass M changes proportionally to the energy density ρ and is not a suitable candidate for a Lagrangian variable. Therefore, we take the Lagrangian grid of M_0, which means we need to find an expression that relates δM_i to δr_i. To derive a description of δM_i depending on δr_i, we are using a similar logic as for the Volume difference ΔV. The conservation of gravitational mass can be discretized as:

$$\frac{\mathrm{d}M}{\mathrm{d}r} = r^2\rho \tag{130}$$

$$\Rightarrow \Delta M_i = \rho_i \frac{r_i^3 - r_{i-1}^3}{3} \tag{131}$$

The perturbation then becomes:

$$\begin{aligned}
\frac{\delta(\Delta M_i)}{\Delta M_i} &= \frac{\delta\rho_i}{\rho_i} + \frac{3r_i^2\delta r_i - 3r_{i-1}^2\delta r_{i-1}}{r_i^3 - r_{i-1}^3} \\
&= \frac{3r_i^2\delta r_i - 3r_{i-1}^2\delta r_{i-1}}{r_i^3 - r_{i-1}^3} - \left(1 + \frac{P_i}{\rho_i}x\right)\frac{\delta(\Delta V_i)}{\Delta V_i} \\
&= -\frac{P_i}{\rho_i}x \cdot \frac{3r_i^2\delta r_i - 3r_{i-1}^2\delta r_{i-1}}{r_i^3 - r_{i-1}^3} - \left(1 + \frac{P_i}{\rho_i}x\right)\left[\frac{x\delta\bar{M}_i}{\bar{r}_i - 2x\bar{M}_i} - \frac{\delta\bar{r}_i}{\bar{r}_i} \cdot \frac{x\bar{M}_i}{\bar{r}_i - 2x\bar{M}_i}\right]
\end{aligned}$$

It is not possible to resolve δM_i as a pure function of δr_{i-1}, δr_i and δr_{i+1}. This makes sense if we remember that M is the enclosed mass and therefore δM_i depends on δr_k, where $k \leq i$. Though it is possible to find a recursive statement about δM_i. Next, we define an auxiliary variable ζ_i and use equation (131).

$$\zeta_i \equiv \frac{1}{2}\left(1 + \frac{P_i}{\rho_i}x\right)\frac{x\Delta M_i}{\bar{r}_i - 2x\bar{M}_i} = \frac{\rho_i + xP_i}{\bar{r}_i - 2x\bar{M}_i} \cdot x\frac{r_i^3 - r_{i-1}^3}{6} \tag{132}$$

$$\delta(\Delta M_i) + 2\zeta_i\delta\bar{M}_i = -P_i\frac{x\Delta M_i}{\rho_i} \cdot \frac{3r_i^2\delta r_i - 3r_{i-1}^2\delta r_{i-1}}{r_i^3 - r_{i-1}^3} + 2\zeta_i\bar{M}_i\frac{\delta\bar{r}_i}{\bar{r}_i}$$

$$\delta M_i\left(\zeta_i + 1\right) + \delta M_{i-1}\left(\zeta_i - 1\right) = -xP_i\left(r_i^2\delta r_i - r_{i-1}^2\delta r_{i-1}\right) + 2\zeta_i\bar{M}_i\frac{\delta\bar{r}_i}{\bar{r}_i}$$

$$\delta M_i = \frac{1 - \zeta_i}{1 + \zeta_i}\delta M_{i-1} - \frac{xP_i}{1 + \zeta_i}\left(r_i^2\delta r_i - r_{i-1}^2\delta r_{i-1}\right) + 2\bar{M}_i\frac{\zeta_i}{1 + \zeta_i}\frac{\delta\bar{r}_i}{\bar{r}_i} \tag{133}$$

The recursive form of the shell-mass perturbation can then be written as

$$\delta M_i = \varepsilon_i \delta M_{i-1} + \alpha_i \delta r_{i-1} + \beta_i \delta r_i, \tag{134}$$

with these auxiliary functions:

$$\zeta_i \equiv \frac{\rho_i + x P_i}{\bar{r}_i - 2x\bar{M}_i} \cdot x \frac{r_i^3 - r_{i-1}^3}{6} \tag{135}$$

$$\varepsilon_i \equiv \frac{1-\zeta_i}{1+\zeta_i} \tag{136}$$

$$\alpha_i \equiv \frac{\bar{M}_i}{\bar{r}_i}\frac{\zeta_i}{1+\zeta_i} + \frac{x P_i r_{i-1}^2}{1+\zeta_i} \tag{137}$$

$$\beta_i \equiv \frac{\bar{M}_i}{\bar{r}_i}\frac{\zeta_i}{1+\zeta_i} - \frac{x P_i r_i^2}{1+\zeta_i} \tag{138}$$

We can imagine this as a linear problem

$$\delta M_i = (L_M)_i{}^j \, \delta r_j, \tag{139}$$

where L_M is a lower triangular matrix, whose elements can be calculated by

$$(L_M)_i{}^j = \sum_{k=0}^{i} \mathrm{inv}\left(\delta_i{}^k - \varepsilon_i \delta_{i-1}{}^k\right)\left(\alpha_k \delta_{k-1}{}^j + \beta_k \delta_k{}^j\right) \tag{140}$$

$$= \sum_{k=0}^{i} \left[\left(\alpha_k \delta_{k-1}{}^j + \beta_k \delta_k{}^j\right) \prod_{p=k+1}^{i} \varepsilon_p\right], \tag{141}$$

but usually this is not needed, because (134) can be used to compute $y_i = (L_M)_i{}^j x_j$ without storing the matrix as implemented in Listing 2.

```
@njit
def apply_LM_to_x(alp, bet, eps, x, y): # computes y = L_M @ x
    n = x.size
    y[0] = alp[0] * x[0]
    for i in range(1, n):
        y[i] = eps[i]*y[i-1] + alp[i]*x[i-1] + bet[i]*x[i]
```

Listing 2: Function that is used to apply $\boldsymbol{L}_M$ to an array x.

By using the derived definitions of δP and $\delta\rho$, the perturbation of the residual is

$$\delta\mathcal{R}_i = a_i \delta r_{i-1} + b_i \delta r_i + c_i \delta r_{i+1} + u_i \delta M_{i-1} + v_i \delta M_i + w_i \delta M_{i+1}, \tag{142}$$

with coefficients

$$\begin{aligned} a_i &\equiv \frac{\partial(\delta\mathcal{R}_i)}{\partial(\delta r_{i-1})}, \quad & b_i &\equiv \frac{\partial(\delta\mathcal{R}_i)}{\partial(\delta r_i)}, \quad & c_i &\equiv \frac{\partial(\delta\mathcal{R}_i)}{\partial(\delta r_{i+1})} \\ u_i &\equiv \frac{\partial(\delta\mathcal{R}_i)}{\partial(\delta M_{i-1})}, \quad & v_i &\equiv \frac{\partial(\delta\mathcal{R}_i)}{\partial(\delta M_i)}, \quad & w_i &\equiv \frac{\partial(\delta\mathcal{R}_i)}{\partial(\delta M_{i+1})}. \end{aligned} \tag{143}$$

Because the expression (117) is quite complex, these coefficients are calculated symbolically using SymPy, a Python library for symbolic mathematics [25]. Note that the coefficients u_i, v_i, w_i vanish in the Newtonian case. The elements δM_i and δM_{i+1} are removed by using the recursive statement (134). Therefore, we can write the Residual in the form

$$\delta\mathcal{R}_i = A_i \delta r_{i-1} + B_i \delta r_i + C_i \delta r_{i+1} + Z_i \delta M_{i-1}, \tag{144}$$

by using the coefficients

$$A_i = a_i + \alpha_i(v_i + w_i\varepsilon_{i+1}), \tag{145}$$
$$B_i = b_i + \beta_i(v_i + w_i\varepsilon_{i+1}) + w_i\alpha_{i+1}, \tag{146}$$
$$C_i = c_i + w_i\beta_{i+1}, \tag{147}$$
$$Z_i = u_i + \varepsilon_i(v_i + w_i\varepsilon_{i+1}). \tag{148}$$

This results in a linear problem of the form

$$\mathcal{R}_i + (\boldsymbol{T} + \boldsymbol{L})_i{}^j\, \delta r_j = 0, \tag{149}$$

where $\boldsymbol{T}$ is a tridiagonal matrix with the subdiagonal A_i, diagonal B_i and superdiagonal C_i, and $\boldsymbol{L}$ is a lower triangular matrix. The elements of $\boldsymbol{L}$ can be computed by

$$L_i{}^j = Z_i(L_M)_{i-1}{}^j, \tag{150}$$

but again, it is not really necessary to store the matrix $\boldsymbol{L}$. We use the recursive definition of δM (134) to apply $L_i{}^j$ to δr_j as in Listing 3.

```
@njit
def apply_L_to_x(Z, alp, bet, eps, x, y): # computes y = L @ x
    apply_LM_to_x(alp, bet, eps, x, y)  # y = LM @ x
    n = x.size
    for i in range(n-1, 0, -1):
        y[i] = Z[i-1] * y[i-1]
    y[0] = 0
```

Listing 3: Function that is used to apply $\boldsymbol{L}$ to an array x.

5.5 Solving the linear problem

We were able to define the linear problem

$$(\boldsymbol{T} + \boldsymbol{L})_i{}^j\, \delta r_j = d_i, \tag{151}$$

where $d_i = -\mathcal{R}_i$. For the Newtonian case, the matrix $\boldsymbol{L}$ vanishes. Assuming that our system is weakly relativistic $\nu < c$, the values of Z, ε, u, v, and w are going to be smaller than the elements of $\boldsymbol{T}$. Thus, the matrix $\boldsymbol{J} = \boldsymbol{T} + \boldsymbol{L}$ is dominantly tridiagonal. To solve this linear problem, I will use $\boldsymbol{T}$ as a preconditioner, i.e., an approximation for $\boldsymbol{J}$, because it is easy to invert a tridiagonal matrix using the tridiagonal matrix algorithm (TDMA). We implement an in-place and split variant of the tridag routine in Numerical Recipes [28]. The forward elimination (LU factorization) is implemented in `TDMA_forward_step` and the forward- and back-substitution is implemented in `TDMA_backward_step`.

```
import numpy as np

@njit
def TDMA_forward_step(a, b, c):
    n = b.size
    for it in range(1, n):
        a[it-1] = a[it-1] / b[it-1]
        b[it] -= a[it-1] * c[it-1]
    return

```

```
@njit
def TDMA_backward_step(a, b, c, d):
    n = d.size
    for it in range(1, n):
        d[it] -= a[it-1] * d[it-1]
    x = np.empty(n, dtype=d.dtype)
    x[-1] = d[-1] / b[-1]
    for it in range(n-2, -1, -1):
        x[it] = (d[it] - c[it] * x[it+1]) / b[it]
    return x
```

Listing 4: TDMA solver split into 'forward' factorization step and 'backwards' solver step.

This approach scales with $\mathcal{O}(n)$, and in the Newtonian case, suffices to solve the linear problem. In the relativistic case, $\boldsymbol{L}$ must be included in the algorithm, even if it is small. A full matrix inversion, which scales as $\mathcal{O}(n^3)$, would significantly increase computational cost. Instead, the system's strong tridiagonality is exploited by employing an iterative linear solver with preconditioning. The preconditioned first-order stationary iterative method, as described in Chapter 5.2 of Iterative Solution Methods [29], is introduced. Consider a linear problem of the form

$$\boldsymbol{A}x = b, \tag{152}$$

with the preconditioner $\boldsymbol{C}$, which approximates $\boldsymbol{A}$, then

$$\boldsymbol{C}\left(x^{k+1} - x^k\right) = -\tau_k\left(\boldsymbol{A}x^k - b\right), \tag{153}$$

is the preconditioned iterative approximation of the solution, where k is the iteration step and τ_k is a relaxation parameter. If $\tau_k = \tau\ \forall k$, then it is called stationary. Restructuring to get an iterative statement yields

$$x^{k+1} = x^k + \tau_k \boldsymbol{C}^{-1}\left(b - \boldsymbol{A}x^k\right) \tag{154}$$

If we use $\tau_k = 1\ \forall k$ and apply this to our system, we get:

$$x^{k+1} = \boldsymbol{T}^{-1}\left(d - \boldsymbol{L}x^k\right). \tag{155}$$

Ensuring convergence of this method is nontrivial, as it requires approximating the eigenvalues of $\boldsymbol{T}^{-1}\boldsymbol{L}$. Therefore, a slower but robust fallback method, the Generalized Minimum Residual Method (GMRES), as described in [30, 31], is employed. The implementation utilizes the routine `scipy.sparse.linalg.gmres` from the SciPy library [24]. The fallback is used if the 2-norm of the residual $||l||_2 > \epsilon$ for a threshold $\epsilon \ll 1$ after a maximum number of iterations `max_iter`. The residual is

$$l^{k+1} = d - (\boldsymbol{T} + \boldsymbol{L})x^{k+1} = \boldsymbol{L}x^k - \boldsymbol{L}x^{k+1}, \tag{156}$$

where we used $d = \boldsymbol{T}x^{k+1} + \boldsymbol{L}x^k$ from rewriting (155). The result of these linear solvers is an array of δr_i. An array of δM_i can be calculated by using (134). The values of δr_i and δM_i can then be plugged into (120), (127), and (129) in order to get updated variables for ρ_0, P and ρ.

```
@njit
def preconditioned_iterative_solver(A, B, C, Z, alp, bet, eps, D,
    max_iter=10, tol=1e-10):
    # Iteratively solves (T+L)x = D
    TDMA_forward_step(A, B, C)
    n = D.size
    x = np.zeros(n)
    rhs = np.empty(n, dtype=D.dtype)
    Lx = np.empty(n, dtype=D.dtype)
    Lx_new = np.empty(n, dtype=D.dtype)
    relres = 1e300

    nd2 = 0.0
    for i in range(n):
        nd2 += D[i]*D[i]
    if nd2 == 0.0:
        nd2 = 1.0

    apply_L_to_x(Z, alp, bet, eps, x, Lx)
    for it in range(max_iter):
        for i in range(n):
            rhs[i] = D[i] - Lx[i]
        x_new = TDMA_backward_step(A, B, C, rhs)
        apply_L_to_x(Z, alp, bet, eps, x_new, Lx_new)
        nr2 = 0.0
        for i in range(n):
            diff = Lx[i] - Lx_new[i]
            nr2 += diff*diff
        relres = np.sqrt(nr2/nd2)
        if relres < tol:
            return x_new, relres
        x = x_new
        Lx, Lx_new = Lx_new, Lx

    return x, relres
```

Listing 5: Fixed point iteration scheme to calculate $(\boldsymbol{T} + \boldsymbol{L})\delta r = -\mathcal{R}$

5.6 Updating Variables

After the desired equilibrium is reached, the variables needed for Heat conduction need to be updated.

$$u_i = \frac{3P_i}{2\rho_{0,i}} \tag{157}$$

$$\gamma_i = xu_i + \sqrt{x^2u_i^2 + 1} \tag{158}$$

$$\rho_i = \gamma_i \cdot \rho_{0,i} \tag{159}$$

$$\nu_i = \sqrt{\frac{P_i}{\rho_i}} \tag{160}$$

$$\mathrm{e}^{\lambda} = \sqrt{\frac{r_i}{r_i - 2M_i x}} \tag{161}$$

$$\phi_{\mathrm{end}} = \frac{1}{2}\ln\left(1 - \frac{2M_{\mathrm{end}}x}{r_{\mathrm{end}}}\right) \tag{162}$$

$$\Delta\phi_i = \frac{x\left(\bar{M}_i + x\bar{r}_i^3 P_i\right)\Delta r_i}{\bar{r}_i\left(\bar{r}_i - 2\bar{M}_i x\right)} \tag{163}$$

$$\phi_i = \phi_{\mathrm{end}} - \sum_{k=1}^{N-1}\Delta\phi_k + \sum_{k=1}^{i}\Delta\phi_k = \phi_{\mathrm{end}} - \sum_{k=i+1}^{N-1}\Delta\phi_k \tag{164}$$

The discrete form of the Luminosity (71) is

$$L_i = -r_i^2\mathrm{e}^{\phi_i}\frac{\kappa_i + \kappa_{i+1}}{2\mathrm{e}^{\lambda_i}}\frac{T_{i+1}\mathrm{e}^{\frac{\phi_{i+1}+\phi_i}{2}} - T_i\mathrm{e}^{\frac{\phi_i+\phi_{i-1}}{2}}}{(r_{i+1} - r_{i-1})/2} \tag{165}$$

or

$$L_i = -r_i^2\mathrm{e}^{3\phi_i/2}\frac{K_{\mathrm{eff},i} + K_{\mathrm{eff},i+1}}{\mathrm{e}^{\lambda_i}}\frac{u_{i+1}\mathrm{e}^{\phi_{i+1}/2} - u_i\mathrm{e}^{\phi_{i-1}/2}}{r_{i+1} - r_{i-1}}, \tag{166}$$

where $T = \frac{2m}{3k_{\mathrm{B}}}u$ and $K_{\mathrm{eff}} = \frac{2m}{3k_{\mathrm{B}}}\kappa$.

6 Simulations

Using the modified code, a set of 2 halo parameters ρ_s, r_s with five different values for σ_m are simulated with $N = 400$ shells, $r_{\min}/r_s = 0.01$ and $r_{\max}/r_s = 15$. This yields 10 halo configurations, each simulated twice: once for the Newtonian and once for the GR case. The 10 halo configurations are labeled as `haloNNN`α with the run index `NNN` and suffix α, which denotes Newtonian $\alpha =$ `a` and GR simulations $\alpha =$ `b`. Indices 001-005 correspond to the first (ρ_s, r_s) pair and 006-010 to the second, while σ_m increases with `NNN` as listed in Table 1.

Table 1: Halo model parameters used in the simulations. The run index `NNN` refers to the directory name `haloNNN`α, where $\alpha =$ `a` (Newtonian) or $\alpha =$ `b` (GR).

Run index `NNN`	ρ_s [$\mathrm{M_\odot\,pc^{-3}}$]	r_s [kpc]
001-005	0.044175	1.28
006-010	0.0194	2.586

Run index `NNN`	σ_m [$\mathrm{cm^2/g}$]
001, 006	0.1
002, 007	1
003, 008	10
004, 009	30
005, 010	80

Figures 2 and 3 show the time evolution at five points in time $\tilde{t}/\tilde{t}_{\mathrm{max}} \in \{0,\, 0.001,\, 0.5,\, 0.99,\, 1.0\}$ for the halos `halo003` and `halo004` with parameters $\rho_s = 0.044\,175\,\mathrm{M_\odot\,pc^{-3}}$, $r_s = 1.28\,\mathrm{kpc}$. They show the typical evolution of the gravothermal collapse, starting with the cuspy NFW profile and quickly producing a cored profile. The radius of the innermost shell increases in this phase, indicating that the core expands. This phase lasts about half the total time until a minimum density is reached and the core becomes isothermal. Afterwards, it continues to heat and slowly collapses. Between the last two timesteps, the energy density increases rapidly in the centre by around two orders of magnitude, from $\tilde{\rho}(\tilde{t}/\tilde{t}_{\mathrm{max}} = 0.99) \approx 1 \times 10^2$ to $\tilde{\rho}(\tilde{t}/\tilde{t}_{\mathrm{max}} = 1.00) \approx 1 \times 10^4$, over a time difference of only 1% of the maximum time.

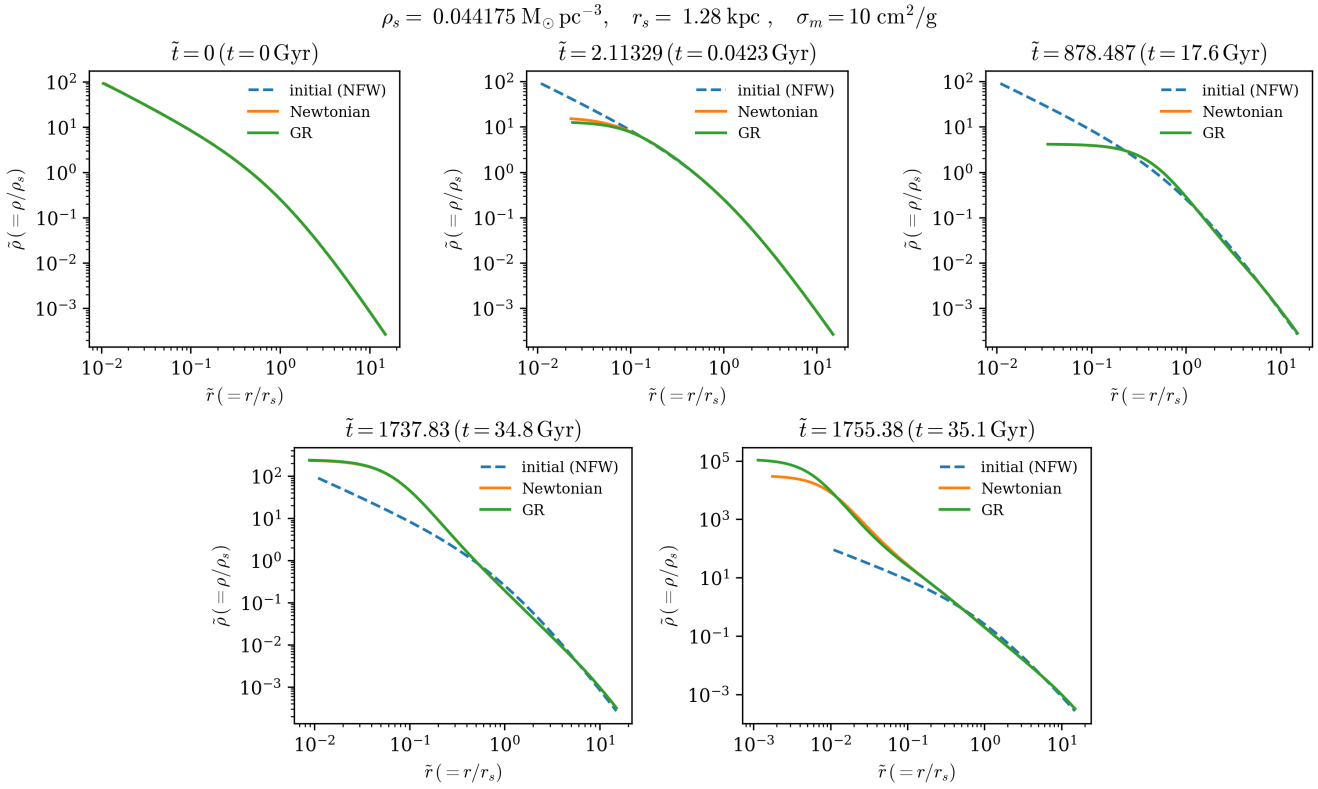

Figure 2: Density profiles of `halo003a` and `halo003b` for times $\tilde{t}/\tilde{t}_{\mathrm{max}} = 0, 0.001, 0.5, 0.99, 1.0$.

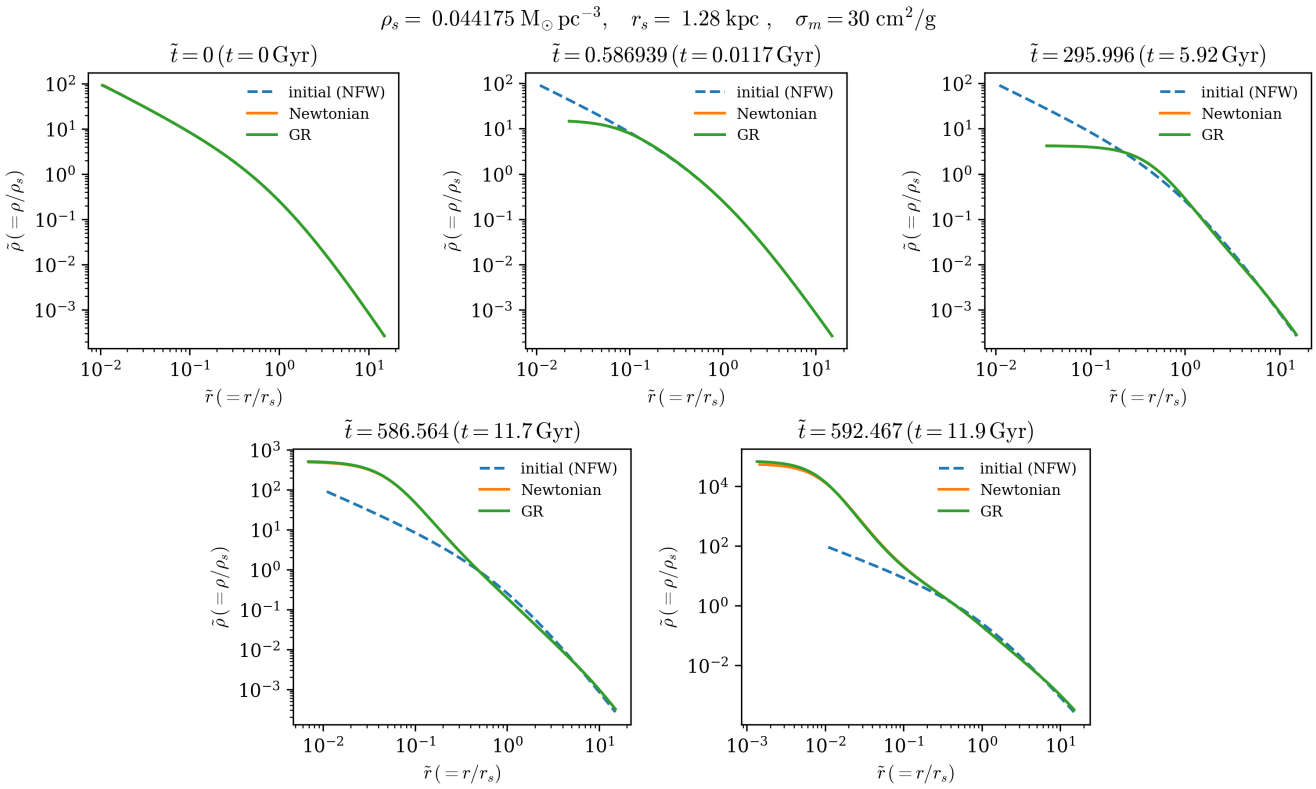

Figure 3: Density profiles of `halo004a` and `halo004b` for times $\tilde{t}/\tilde{t}_{\max} = 0, 0.001, 0.5, 0.99, 1.0$.

The key difference between the final profiles of `halo003` and `halo004` is that in the first case with $\sigma_m = 10\,\mathrm{cm}^2/\mathrm{g}$, the central density is significantly larger in the relativistic simulation, by around an order of magnitude, and only marginally larger for `halo004` with $\sigma_m = 30\,\mathrm{cm}^2/\mathrm{g}$. Up to the collapse phase, we can't distinguish between the GR and Newtonian simulations. This is expected if the code works as intended.

The final halo profiles for all values of the cross-section are shown in Figure 4 for the first halo and in Figure 5 for the second halo. For smaller values of σ_m, the halo evolution is slower, resulting in longer times in the range of hundreds of Gyrs. The simulations also run slower, which is why no collapse was reached for $\sigma_m = 1\,\mathrm{cm}^2/\mathrm{g}$ and $\sigma_m = 0.1\,\mathrm{cm}^2/\mathrm{g}$ over a simulation runtime of ≈ 3 days. These figures also reveal that the central-density deviation between Newtonian and GR vanishes for larger σ_m in both halos.

Another visualization of the evolution in Figure 6 shows the central density of the five halos `halo001b` to `halo005b` as a function of a rescaled time variable $\tilde{t}_\sigma = \tilde{t} \cdot \sigma_M/(100\,\mathrm{cm}^2\,\mathrm{g}^{-1})$. Previously, we noted that smaller values of σ_m correspond to slower time evolution, i.e., larger times. Thus, we scale the time by this factor to align the profiles. Each dot represents a time point of 13 Gyr for the corresponding cross-section. The smaller the cross-section, the earlier in the halo evolution this point is reached. For $\sigma_m = 10, 30, 80\,\mathrm{cm}^2/\mathrm{g}$, the time of 13 Gyr was not reached before the gravothermal collapse.

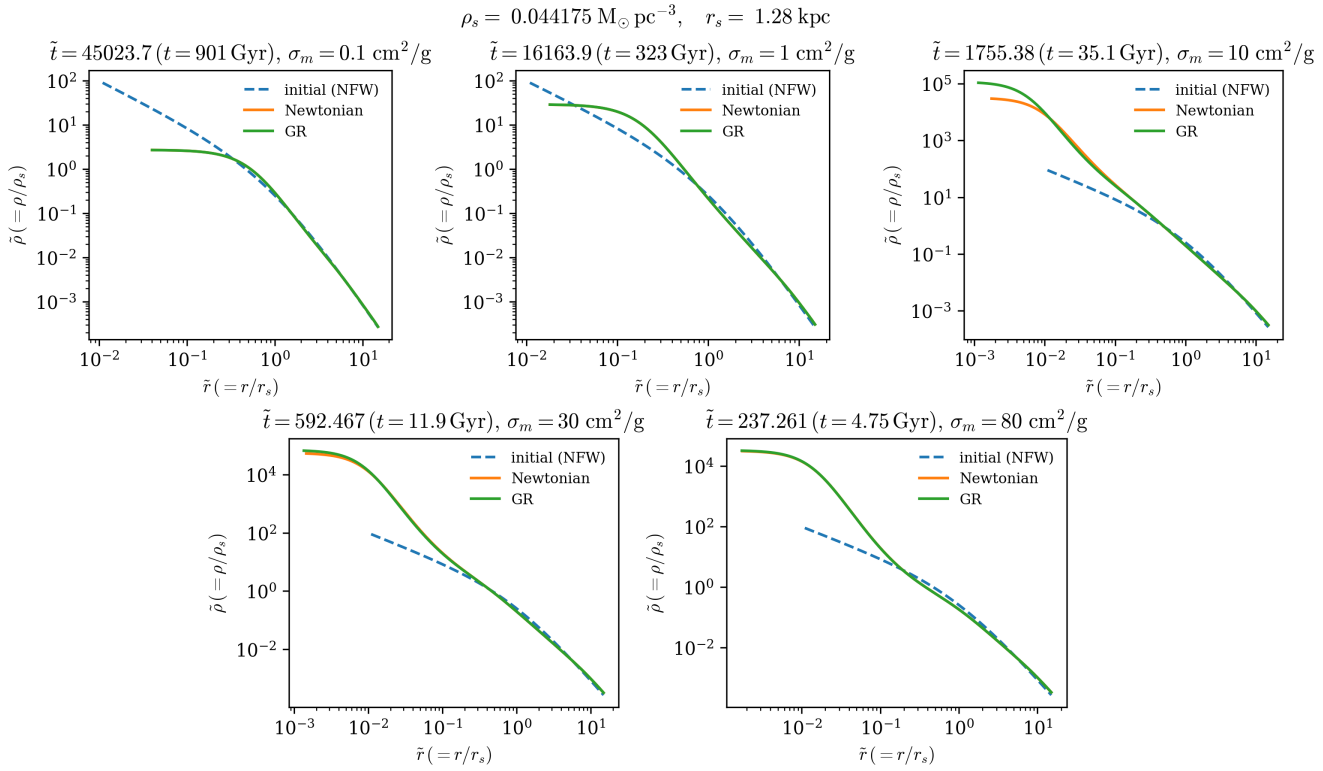

Figure 4: Density profiles of `halo001` to `halo005` for their respective final evolved time $\tilde{t}_{\mathrm{max}}$.

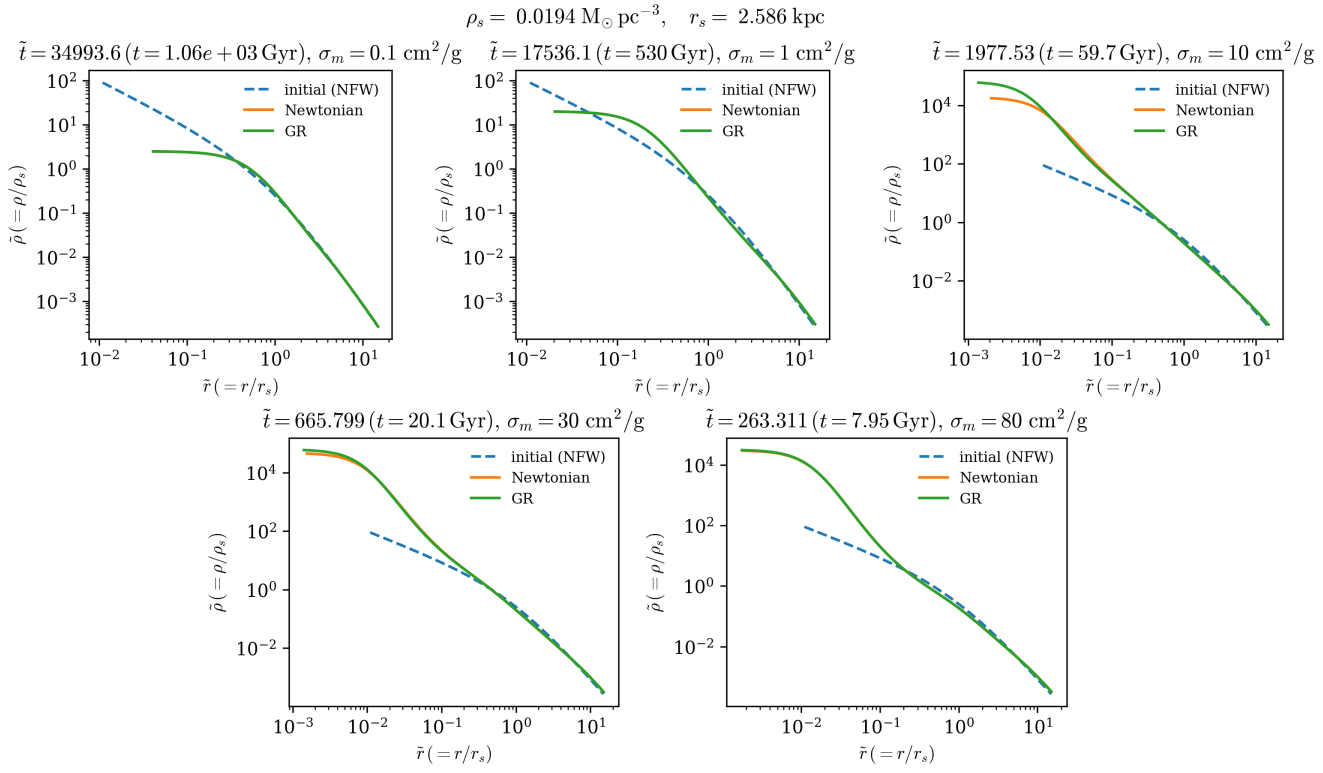

Figure 5: Density profiles of `halo006` to `halo010` for their respective final evolved time $\tilde{t}_{\mathrm{max}}$.

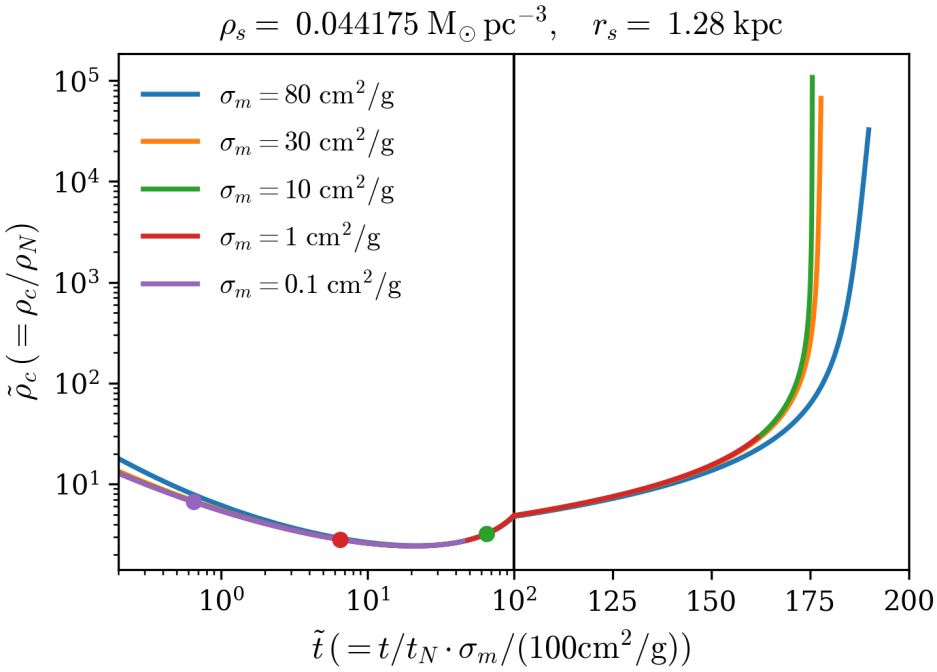

Figure 6: Normalized density profiles $\tilde{\rho}$ of the five cross-sections for `halo001b` to `halo005b` as a function of scaled time $\tilde{t}_\sigma = \tilde{t}\cdot\sigma_M/(100\,\mathrm{cm}^2\,\mathrm{g}^{-1})$. Each dot represents the point where the corresponding cross-section has reached $t = 13\,\mathrm{Gyr}$.

Figure 6 helps in understanding how the evolution differs between cross-sections, but not how the Newtonian simulation differs from the GR simulation. To visualize the difference between the Newtonian and GR runs, the relative difference of the central density $(\rho_{c,\mathrm{GR}} - \rho_{c,\mathrm{Newt}})/\rho_{c,\mathrm{Newt}}$ is shown as a function of scaled time $\tilde{t}_\sigma = \tilde{t}\cdot\sigma_M/(100\,\mathrm{cm}^2\,\mathrm{g}^{-1})$ in Figure 7 for halos `halo001` to `halo005` and in Figure 8 for halos `halo006` to `halo010`.

These figures show a significant difference at the beginning of the simulation, which stems from the fact that, in the GR case, the hydrostatic equilibrium equation must be applied in advance to obtain correct initial conditions. The fluctuations are due to time interpolation because the time steps between the Newtonian and GR cases don't align. Add to that the fact that the larger values of σ_m evolve faster, which leads to a bad temporal resolution at the beginning. Still, we see that for most of the simulation, after the initial phase, the relative difference is in the range of 10^{-4} to 10^{-3} across all cross-sections and in both halos. The time at which the difference increases sharply coincides with the gravothermal collapse. Here, it's apparent that for $\sigma_m = 80\,\mathrm{cm}^2/\mathrm{g}$, the difference flattens and reaches a maximum of around 4×10^{-2}, which fits the earlier observation of the parallel behavior of the Newtonian and GR profiles. For smaller values of σ_m, the difference rises steeply at the gravothermal collapse, without any visible flattening. In Figure 7 the progression of the halo with $\sigma_m = 1\,\mathrm{cm}^2/\mathrm{g}$ follows the general trend of $\sigma_m = 10\,\mathrm{cm}^2/\mathrm{g}$. Extrapolating from that, we could assume that this difference might also rise as rapidly, but longer simulations would be needed to confirm.

The increase in central density during the gravothermal collapse phase is notable, given that the evolution of the Newtonian and general relativistic simulations is nearly identical up to that point. Relativistic effects are expected to become significant only when sufficiently high central densities and velocity dispersions are attained. However, within the scope of this work, it remains inconclusive whether the observed density enhancement

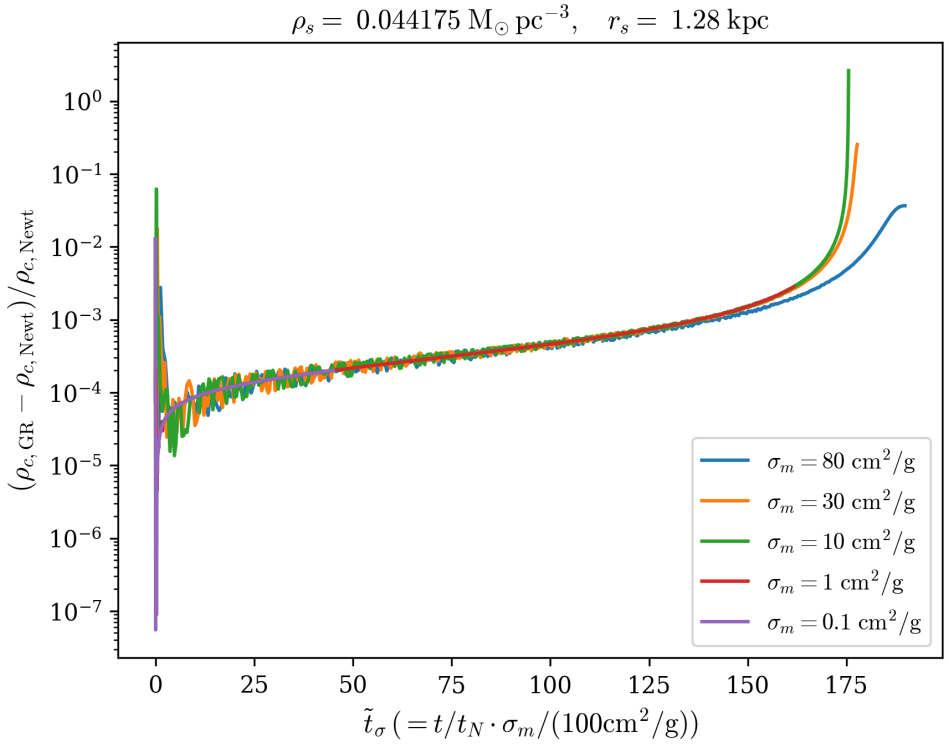

Figure 7: Relative difference of the central densities $(\rho_{c,\mathrm{GR}} - \rho_{c,\mathrm{Newt}})/\rho_{c,\mathrm{Newt}}$ over scaled time $\tilde{t}_\sigma = \tilde{t} \cdot \sigma_M/(100\,\mathrm{cm}^2\,\mathrm{g}^{-1})$ of `halo001` to `halo005`.

.

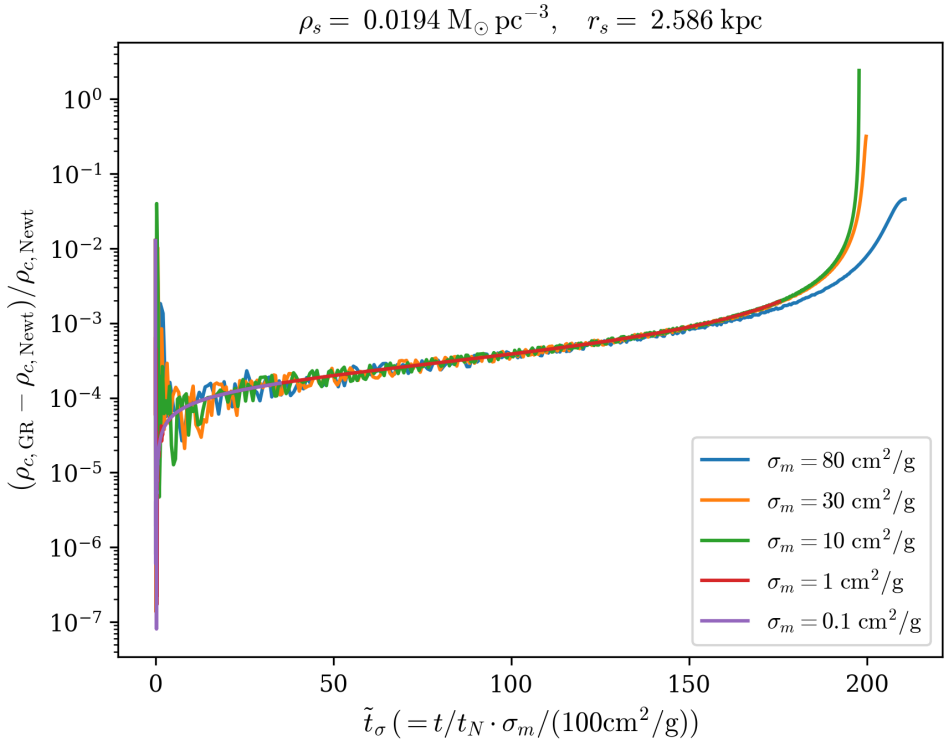

Figure 8: Relative difference of the central densities $(\rho_{c,\mathrm{GR}} - \rho_{c,\mathrm{Newt}})/\rho_{c,\mathrm{Newt}}$ over scaled time $\tilde{t}_\sigma = \tilde{t} \cdot \sigma_M/(100\,\mathrm{cm}^2\,\mathrm{g}^{-1})$ of `halo006` to `halo010`.

.

is a genuine physical effect or is partially influenced by numerical limitations, such as finite spatial resolution, timestep control, or the treatment of heat transport, as most of the time was devoted to developing the underlying code.

To determine whether these results are numerical artifacts, further simulations with a higher shell number $N > 400$ and/or a smaller inner radius $\tilde{r}_{\min} < 0.01$ would be required. If the central densities between the Newtonian and relativistic models converge for larger N or smaller $\tilde{r}_{\min}$, then the utility of semi-analytical models in a general relativistic context for primarily non-relativistic fluids may be limited. Nonetheless, other gravothermal fluids, such as globular clusters, could potentially benefit from this code. Conversely, if the difference between the models is reproduced for larger N and smaller $\tilde{r}_{\min}$, it would be necessary to conduct comparable N-body simulations employing a non-Minkowski background spacetime for comparison. Another important caveat is that the Fourier equation uses an infinite propagation speed for heat conduction. This is obviously not compatible with relativity. Hence, it would be recommended to switch from the parabolic Fourier equation to a hyperbolic heat conduction equation, as discussed by Israel & Stewart [32].

7 Conclusion

In this work, a general-relativistic model of a spherically symmetric self-interacting dark-matter halo was developed using the Tolman-Oppenheimer-Volkoff equations for hydrostatic equilibrium, conservation of mass and energy, and thermodynamic relations. The resulting equations were discretized, solved numerically, and incorporated into an existing numerical framework. Simulations were run with the Newtonian and GR codes for two different halo parameter pairs and five values of σ_m. Gravothermal collapse occurred for both halo parameter pairs with $\sigma_m = 10, 30, 80\,\mathrm{cm}^2/\mathrm{g}$. Here, the general relativistic case produced significantly larger density spikes for $\sigma_m = 10\,\mathrm{cm}^2/\mathrm{g}$, with the difference decreasing as σ_m increased.

Further work could involve running the simulations until the halos with $\sigma_m < 10\,\mathrm{cm}^2/\mathrm{g}$ have collapsed to determine if the observed trend persists. Additionally, more values of σ_m could be run between 1 and $10\,\mathrm{cm}^2/\mathrm{g}$. Increasing N or decreasing $r_{\min}$ could also be considered to assess whether the Newtonian and relativistic solutions converge for smaller σ_m. Finally, implementing a hyperbolic heat-transport equation, such as the one proposed by Israel and Stewart, could address the issue of infinite propagation speed introduced by the parabolic Fourier equation.

References

[1] S. Dodelson. *Modern cosmology*. Amsterdam [u.a.]: Academic Press, 2003, XIII, 440 S.

[2] S. Tulin and H.-B. Yu. "Dark matter self-interactions and small scale structure". In: *Physics Reports* 730 (Feb. 2018), pp. 1–57. DOI: 10.1016/j.physrep.2017.11.004.

[3] D. N. Spergel and P. J. Steinhardt. "Observational Evidence for Self-Interacting Cold Dark Matter". In: *Physical Review Letters* 84.17 (Apr. 2000), pp. 3760–3763. DOI: 10.1103/physrevlett.84.3760.

[4] J. Pollack. "Supermassive Black Holes from Gravothermal Collapse of Fractional Self-Interacting Dark Matter halos". Bachelor thesis. Princeton U., 2012.

[5] N. J. Outmezguine, K. K. Boddy, S. Gad-Nasr, M. Kaplinghat, and L. Sagunski. "Universal gravothermal evolution of isolated self-interacting dark matter halos for velocity-dependent cross-sections". In: *Monthly Notices of the Royal Astronomical Society* 523.3 (June 2023), pp. 4786–4800. DOI: 10.1093/mnras/stad1705.

[6] S. Gad-Nasr, K. K. Boddy, M. Kaplinghat, N. J. Outmezguine, and L. Sagunski. *On the Late-Time Evolution of Velocity-Dependent Self-Interacting Dark Matter Halos*. 2023. arXiv: 2312.09296 [astro-ph.GA].

[7] R. C. Tolman. "Static Solutions of Einstein's Field Equations for Spheres of Fluid". In: *Phys. Rev.* 55 (4 Feb. 1939), pp. 364–373. DOI: 10.1103/PhysRev.55.364.

[8] J. R. Oppenheimer and G. M. Volkoff. "On Massive Neutron Cores". In: *Phys. Rev.* 55 (4 Feb. 1939), pp. 374–381. DOI: 10.1103/PhysRev.55.374.

[9] S. L. Shapiro. "Star clusters, self-interacting dark matter halos, and black hole cusps: The fluid conduction model and its extension to general relativity". In: *Physical Review D* 98.2 (July 2018). DOI: 10.1103/physrevd.98.023021.

[10] N. Aghanim, Y. Akrami, M. Ashdown, et al. "Planck 2018 results: VI. Cosmological parameters". In: *Astronomy amp; Astrophysics* 641 (Sept. 2020), A6. DOI: 10.1051/0004-6361/201833910.

[11] D. J. Fixsen. "THE TEMPERATURE OF THE COSMIC MICROWAVE BACKGROUND". In: *The Astrophysical Journal* 707.2 (Nov. 2009), pp. 916–920. DOI: 10.1088/0004-637x/707/2/916.

[12] D. H. Weinberg, M. J. Mortonson, D. J. Eisenstein, C. Hirata, A. G. Riess, and E. Rozo. "Observational probes of cosmic acceleration". In: *Physics Reports* 530.2 (2013). Observational Probes of Cosmic Acceleration, pp. 87–255. DOI: https://doi.org/10.1016/j.physrep.2013.05.001.

[13] J. F. Navarro, C. S. Frenk, and S. D. M. White. "The Structure of Cold Dark Matter Halos". In: *The Astrophysical Journal* 462 (May 1996), p. 563. DOI: 10.1086/177173.

[14] W. J. G. de Blok. "The Core-Cusp Problem". In: *Advances in Astronomy* 2010.1 (2010), p. 789293. DOI: https://doi.org/10.1155/2010/789293. eprint: https://onlinelibrary.wiley.com/doi/pdf/10.1155/2010/789293.

[15] S.-H. Oh, C. Brook, F. Governato, E. Brinks, L. Mayer, W. J. G. de Blok, A. Brooks, and F. Walter. "THE CENTRAL SLOPE OF DARK MATTER CORES IN DWARF GALAXIES: SIMULATIONS VERSUS THINGS". In: *The Astronomical Journal* 142.1 (June 2011), p. 24. DOI: 10.1088/0004-6256/142/1/24.

[16] F. Walter, E. Brinks, W. J. G. de Blok, F. Bigiel, R. C. Kennicutt, M. D. Thornley, and A. Leroy. "THINGS: THE HI NEARBY GALAXY SURVEY". In: *The Astronomical Journal* 136.6 (Nov. 2008), p. 2563. DOI: 10.1088/0004-6256/136/6/2563.

[17] D. Lynden-Bell and R. Wood. "The Gravo-Thermal Catastrophe in Isothermal Spheres and the Onset of Red-Giant Structure for Stellar Systems". In: *Monthly Notices of the Royal Astronomical Society* 138.4 (Feb. 1968), pp. 495–525. DOI: 10.1093/mnras/138.4.495. eprint: https://academic.oup.com/mnras/article-pdf/138/4/495/8078821/mnras138-0495.pdf.

[18] J. Koda and P. R. Shapiro. "Gravothermal collapse of isolated self-interacting dark matter haloes: N-body simulation versus the fluid model: Gravothermal collapse of isolated SIDM haloes". In: *Monthly Notices of the Royal Astronomical Society* 415.2 (June 2011), pp. 1125–1137. DOI: 10.1111/j.1365-2966.2011.18684.x.

[19] L. Rezzolla and O. Zanotti. *Relativistic Hydrodynamics*. Oxford University Press, Sept. 2013. DOI: 10.1093/acprof:oso/9780198528906.001.0001.

[20] F. Jüttner. *Das Maxwellsche Gesetz der Geschwindigkeitsverteilung in der Relativtheorie*. Jan. 1911. DOI: 10.1002/andp.19113390503.

[21] R. Tolman and P. Ehrenfest. "Temperature Equilibrium in a Static Gravitational Field". In: *Phys. Rev.* 36.12 (1930), pp. 1791–1798. DOI: 10.1103/PhysRev.36.1791.

[22] B. Ram and B. R. Majhi. *General relativistic heat flow from first order hydrodynamics*. 2025. arXiv: 2412.02364 [gr-qc].

[23] C. R. Harris, K. J. Millman, S. J. van der Walt, et al. "Array programming with NumPy". In: *Nature* 585.7825 (Sept. 2020), pp. 357–362. DOI: 10.1038/s41586-020-2649-2.

[24] P. Virtanen, R. Gommers, T. E. Oliphant, et al. "SciPy 1.0: Fundamental Algorithms for Scientific Computing in Python". In: *Nature Methods* 17 (2020), pp. 261–272. DOI: 10.1038/s41592-019-0686-2.

[25] A. Meurer, C. P. Smith, M. Paprocki, et al. "SymPy: symbolic computing in Python". In: *PeerJ Computer Science* 3 (Jan. 2017), e103. DOI: 10.7717/peerj-cs.103.

[26] Astropy Collaboration, A. M. Price-Whelan, P. L. Lim, et al. "The Astropy Project: Sustaining and Growing a Community-oriented Open-source Project and the Latest Major Release (v5.0) of the Core Package". In: 935.2, 167 (Aug. 2022), p. 167. DOI: 10.3847/1538-4357/ac7c74. arXiv: 2206.14220 [astro-ph.IM].

[27] S. K. Lam, A. Pitrou, and S. Seibert. "Numba: a LLVM-based Python JIT compiler". In: *Proceedings of the Second Workshop on the LLVM Compiler Infrastructure in HPC*. LLVM '15. Austin, Texas: Association for Computing Machinery, 2015. DOI: 10.1145/2833157.2833162.

[28] W. H. Press. *Numerical recipes : the art of scientific computing*. 3. ed., this printing is corrected to software version 3.0. Cambridge [u.a.]: Cambridge Univ. Press, 2007, XXI, 1235 S.

[29] O. Axelsson. *Iterative solution methods*. Cambridge, UK: Cambridge University Press, 1994, 1 Online–Ressource (xiii, 654 pages).

[30] Y. Saad. *Iterative methods for sparse linear systems*. 2. ed. Philadelphia: SIAM, 2003, XVIII, 528 S.

[31] Y. Saad and M. H. Schultz. "GMRES: A Generalized Minimal Residual Algorithm for Solving Nonsymmetric Linear Systems". In: *SIAM Journal on Scientific and Statistical Computing* 7.3 (1986), pp. 856–869. DOI: 10.1137/0907058. eprint: https://doi.org/10.1137/0907058.

[32] W. Israel and J. Stewart. "Transient relativistic thermodynamics and kinetic theory". In: *Annals of Physics* 118.2 (1979), pp. 341–372. DOI: https://doi.org/10.1016/0003-4916(79)90130-1.

Ehrenwörtliche Erklärung

An das Ende von schriftlichen Arbeiten (bspw. Seminararbeiten, Bachelor- oder Masterarbeiten) ist eine ehrenwörtliche Erklärung zu setzen. Sie hat folgenden Wortlaut:

Erklärung nach § 30 (12) Ordnung 2013 des FB Physik an der Goethe-Universität für den BAMA-Studiengang Physik

Hiermit erkläre ich, dass ich die Arbeit selbstständig und ohne Benutzung anderer als der angegebenen Quellen und Hilfsmittel verfasst habe. Alle Stellen der Arbeit, die wörtlich oder sinngemäß aus Veröffentlichungen oder aus anderen fremden Texten entnommen wurden, sind von mir als solche kenntlich gemacht worden. Ferner erkläre ich, dass die Arbeit nicht - auch nicht auszugsweise - für eine andere Prüfung oder Studienleistung verwendet wurde.

Zudem versichere ich, dass die von mir eingereichten schriftlichen gebundenen Versionen meiner Bachelorarbeit mit der eingereichten elektronischen Version meiner Bachelorarbeit übereinstimmt.

Frankfurt am Main, den

_____

Unterschrift der/des Studierenden